nature portfolio

https://doi.org/10.1038/s41563-022-01312-3

Supplementary information

Transient nuclear deformation primes epigenetic state and promotes cell reprogramming

In the format provided by the authors and unedited

Supplementary Text

Supplementary Video 1. Video of iN cells generated from mechanical squeezing treatment and labeled with the calcium indicator, Fluo-4 AM, after 6 weeks in culture.

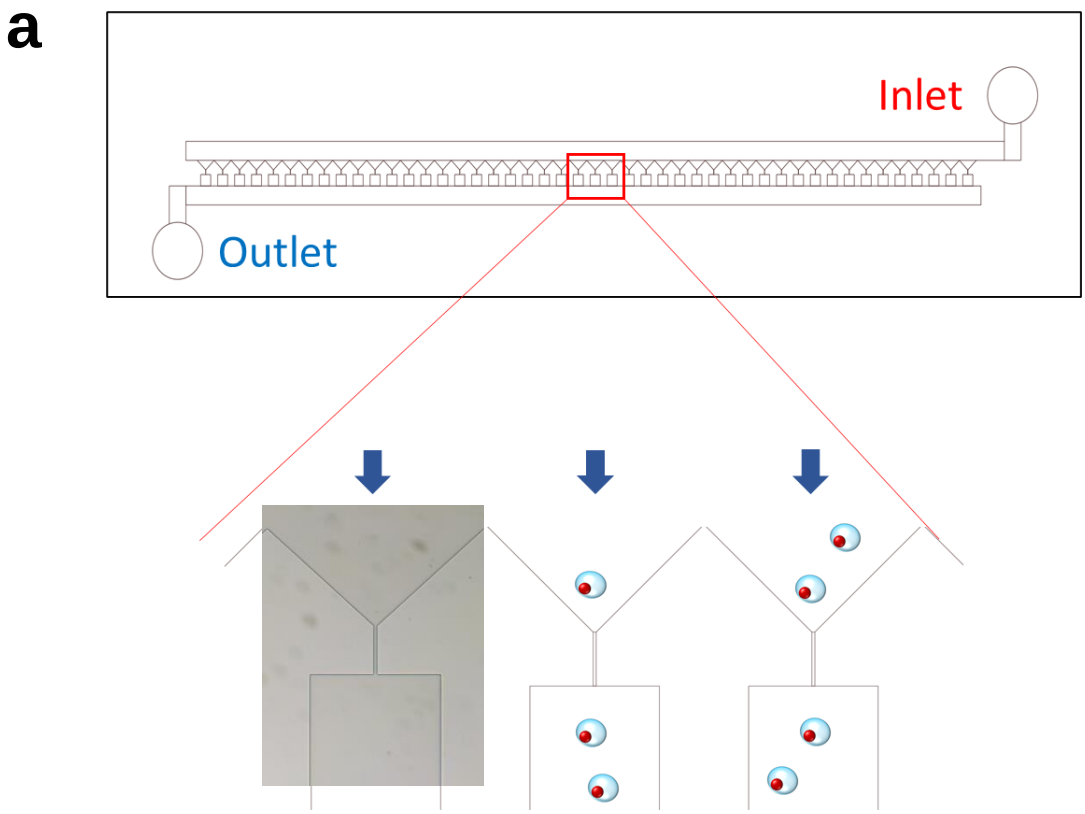

Supplementary Figure 1. A microdevice with parallel microchannels to force transient cell deformation. (a) Schematic illustrating the design of a microdevice with multiple microchannels to deform cells in parallel. **(b)** Mouse fibroblasts were labeled with Cell Tracker Green, and live cell imaging was performed to monitor cells passing through the microchannels. Scale bar, 50 μm.

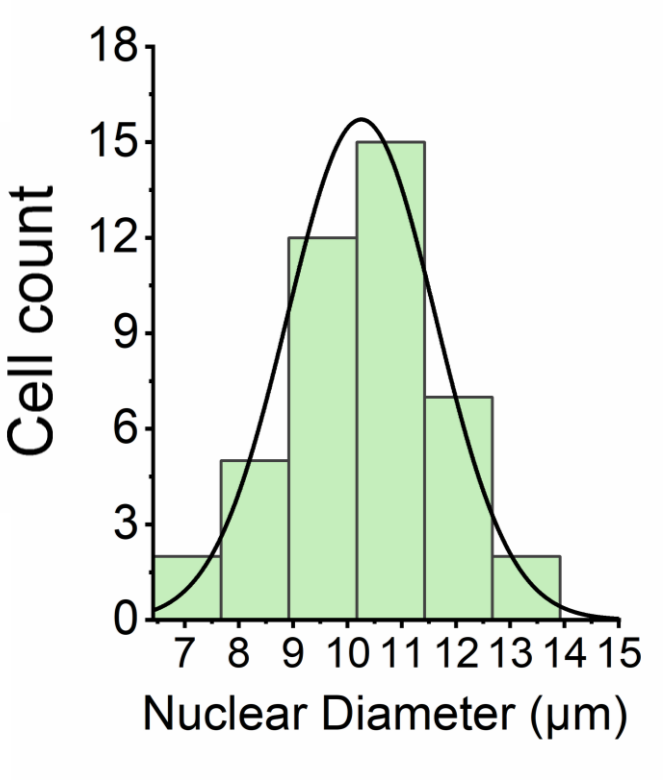

Supplementary Figure 2. **Nuclear diameter of mouse fibroblasts passing through 200-μm channels.** Living cells with stained nuclei (by Hoechst) were introduced into 200-μm channels. Epifluorescence images were collected using a Zeiss Axio Observer Z1 inverted fluorescence microscope. Nuclear diameter was measured using the line tool in the Zen Zeiss software (n=40 cells).

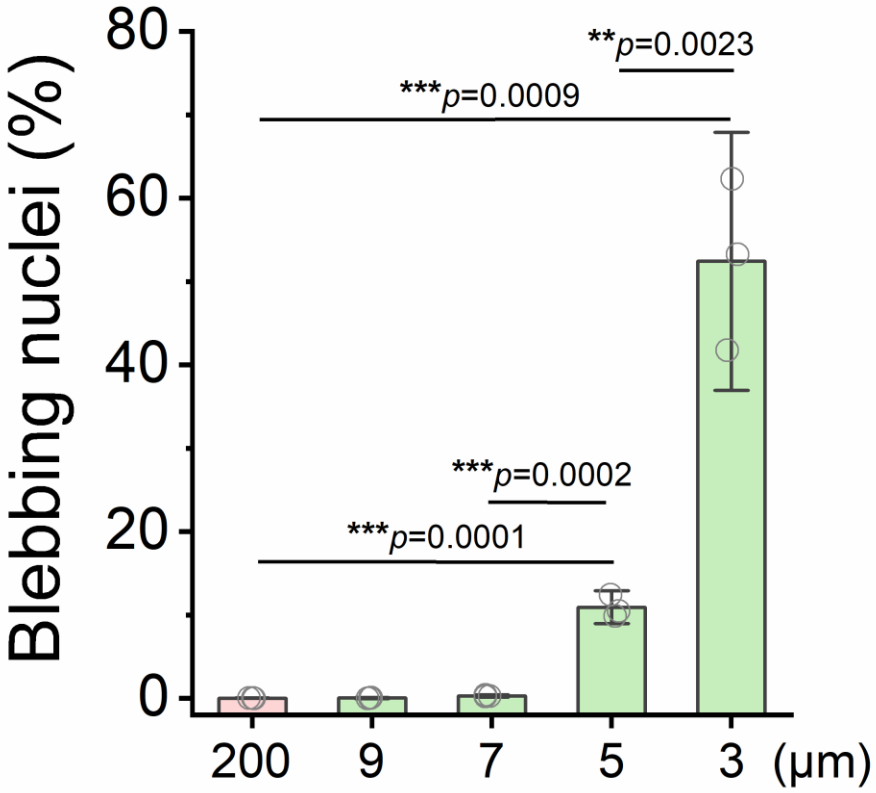

Supplementary Figure 3. Effect of microchannel width on nuclear blebbing. Mouse fibroblasts were introduced into microchannels of various widths, and collected cells were seeded onto fibronectin-coated surfaces, allowed to attached for 3 hours, fixed and stained with DAPI. The percentage of nuclei with blebbing was quantified based on DAPI staining. Each sample includes at least 5,000 cells (n=3). Statistical significance was determined by a one-way ANOVA and Tukey's multiple comparison test. All squeezing groups were compared with the 200-μm group. The data represent the mean ± standard deviation (SD).

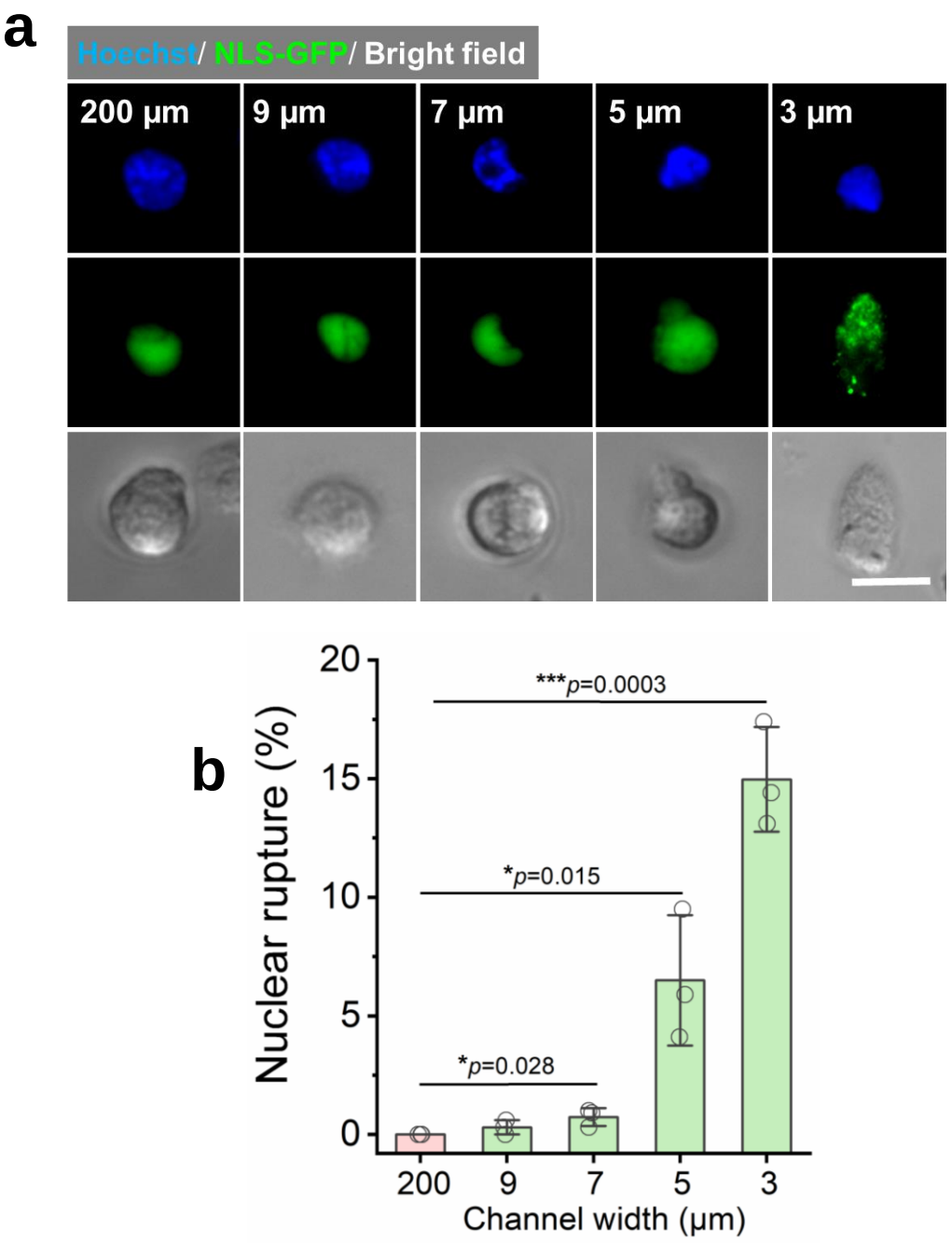

Supplementary Figure 4. Effect of microchannel width on nuclear permeability. **(a)** Mouse fibroblasts were transfected with a nuclear localization signal (NLS)-GFP construct for 72 hours and Hoechst for 30 minutes before being deformed using microchannels with different widths. Cells were imaged immediately after squeezing. Scale bar, 10 µm. **(b)** Quantification of nuclear rupture based on immunofluorescent images (n=3). Statistical significance was determined by a one-way ANOVA and Tukey's multiple comparison test. All squeezing groups were compared with the 200-µm group. The data represent the mean ± SD.

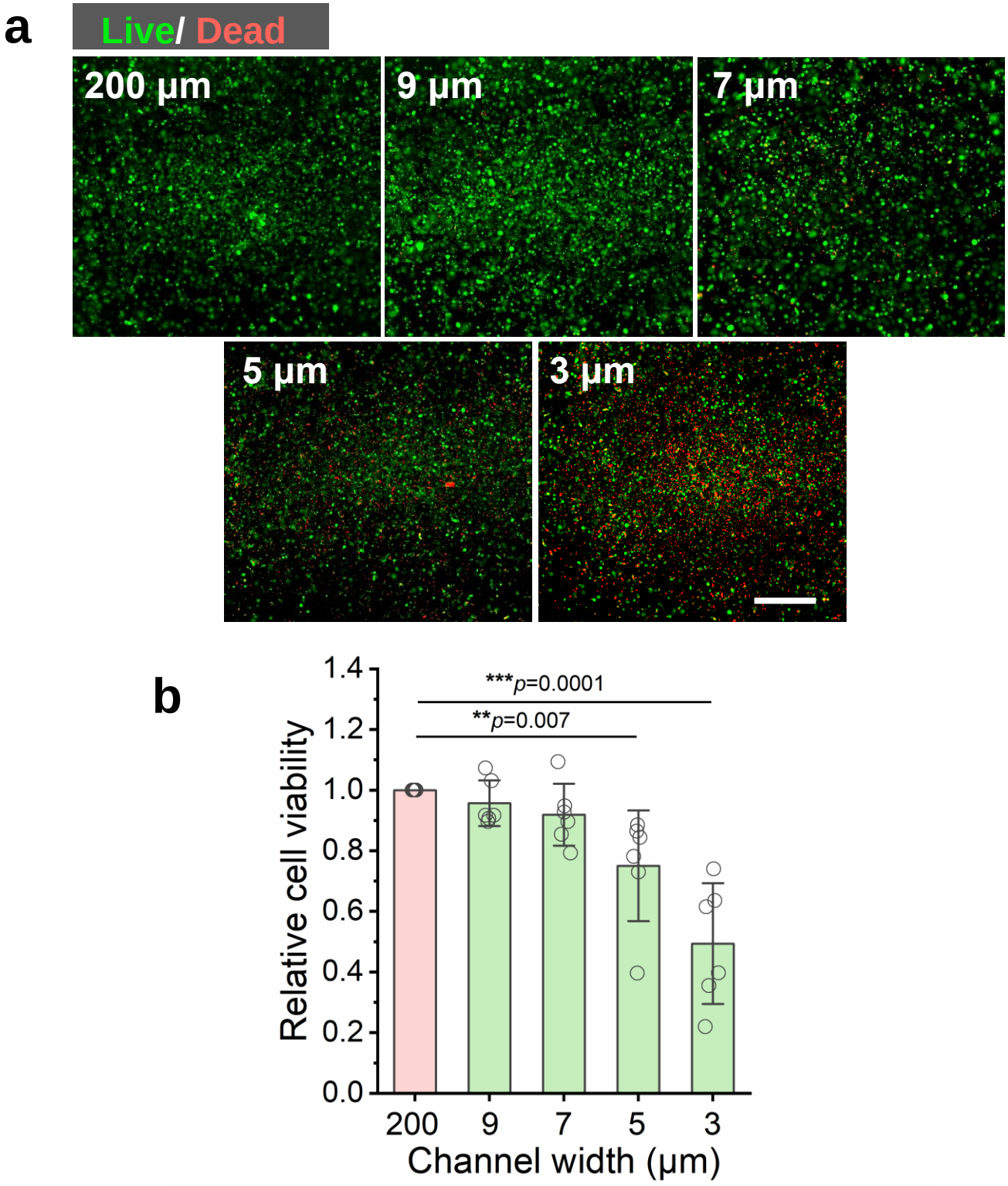

Supplementary Figure 5. Effect of microchannel width on cell viability. (a) Immunofluorescent images show the viability of mouse fibroblasts at 3 hours after passing through microchannels of various widths as determined by the LIVE/DEAD assay. Scale bar, 1 mm. **(b)** Cell viability of fibroblasts at 24 hours after passing through the microchannels of various widths was determined by the PrestoBlue® cell viability assay (n=6). Cell viability was normalized with the control (the viability of cells passing through 200-μm channels). Statistical significance was determined by a one-way ANOVA and Tukey's multiple comparison test. All squeezing groups were compared with the 200-μm group. The data represent the mean ± SD.

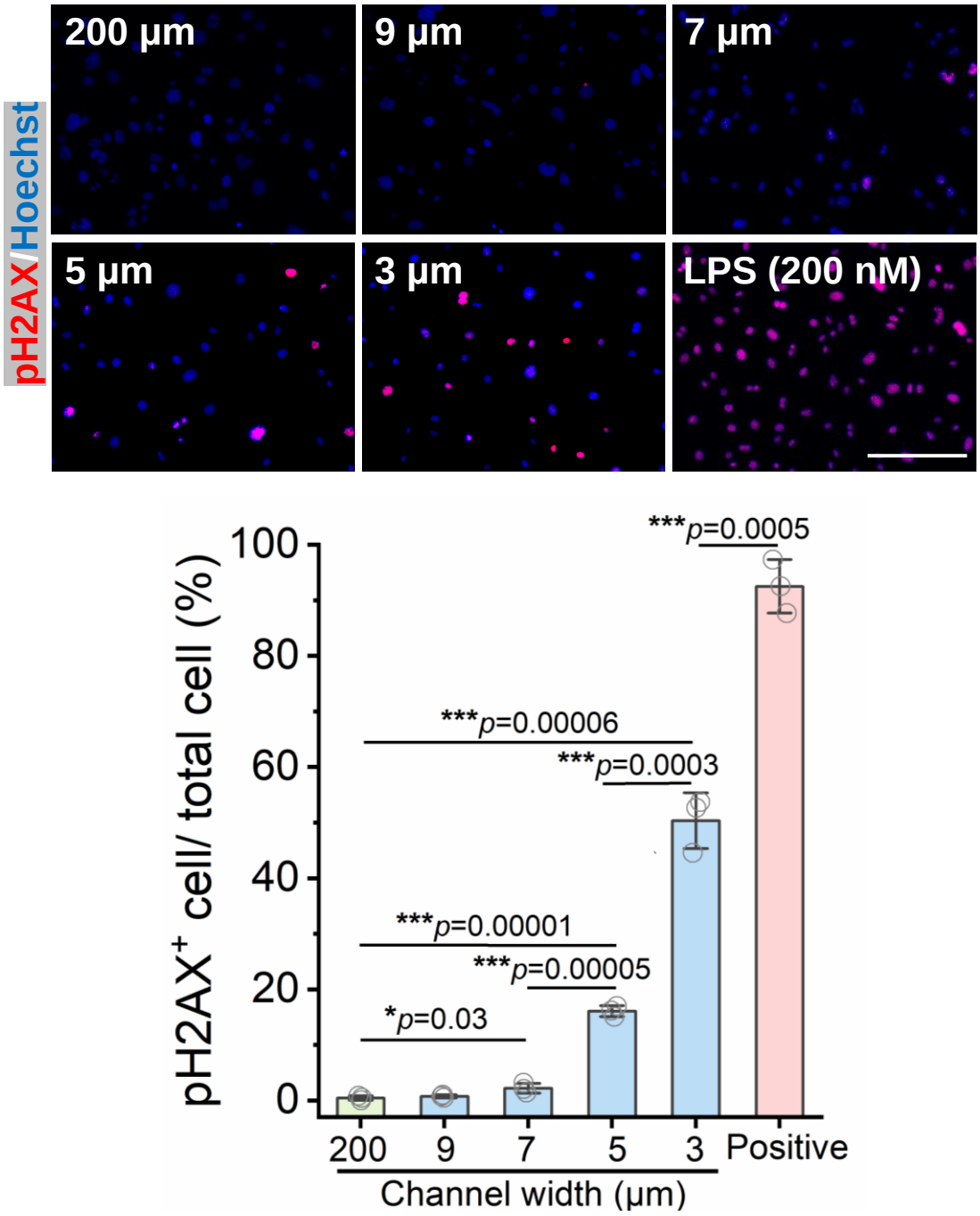

Supplementary Figure 6. Effect of microchannel width on DNA damage. Immunofluorescent images show DNA damage in fibroblasts at 3 hours after passing through microchannels of various widths as determined by the HCS DNA damage assay, where lipopolysaccharide (LPS) at 200 nM was used as a positive control. Scale bar, 100 μm. The percentage of pH2Ax⁺ cells was quantified based on immunofluorescent images (n=3). Statistical significance was determined by a one-way ANOVA and Tukey's multiple comparison test. All squeezing groups were compared with the 200-μm group. The data represent the mean ± SD.

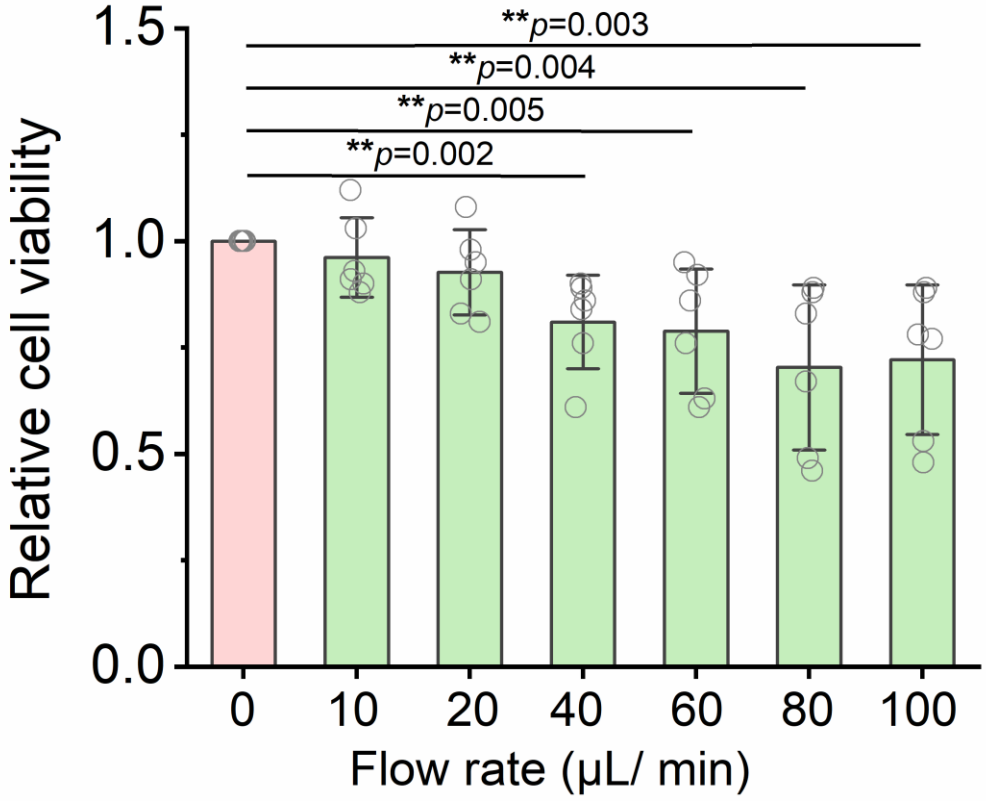

Supplementary Figure 7. Effect of flow rate on cell viability. Mouse fibroblasts were squeezed through 7-μm microchannels with various flow rates or cultured under static condition (set as 0 μL/minute flow rate), seeded on fibronectin-coated surfaces, and allowed to attach for 24 hours. Cell viability was analyzed by PrestoBlue® cell viability assay, and normalized to the static group (n=6). Statistical significance was determined by a one-way ANOVA and Tukey's multiple comparison test. All flow groups were compared with the static group. The data represent the mean ± SD.

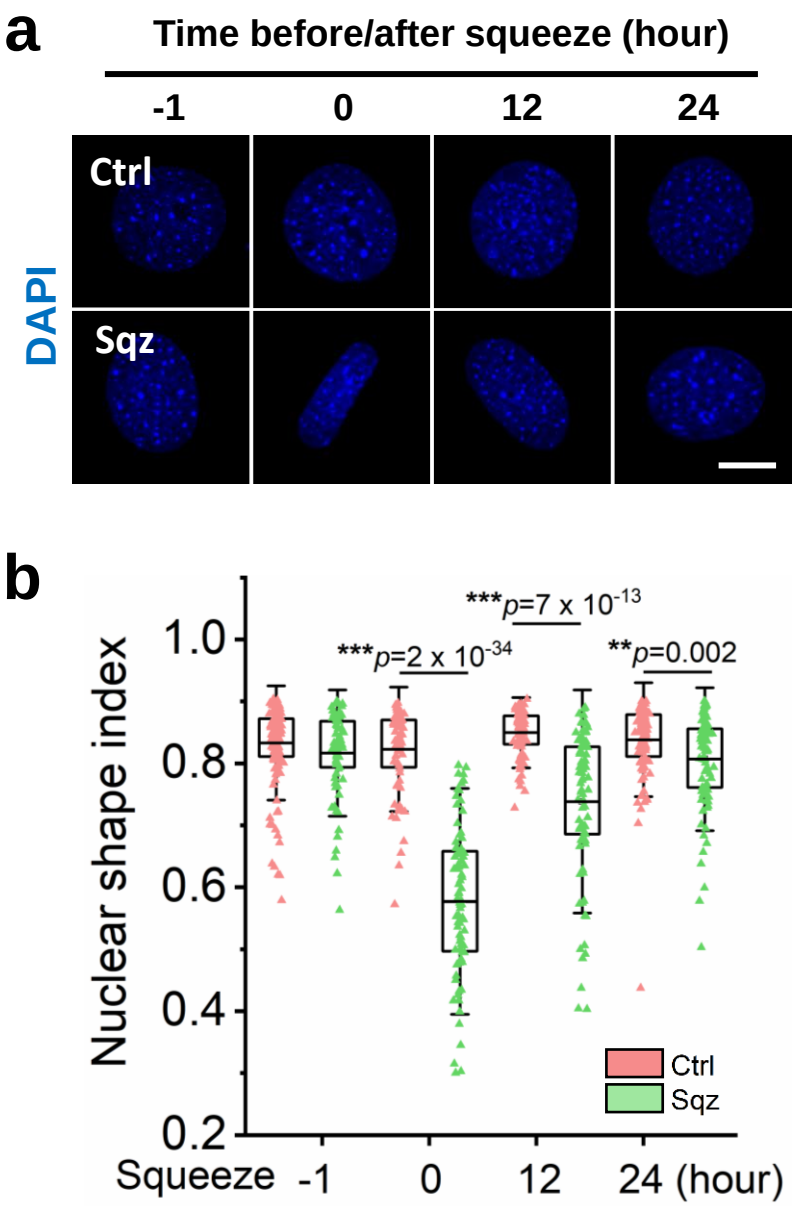

Supplementary Figure 8. Microchannel-induced nuclear morphology changes. (a) Immunofluorescent images of nuclei before and after cells were squeezed through the microchannel. Control (Ctrl): cells passing through 200-μm channels. Squeezed (Sqz): cells passing through 7-μm microchannels. Scale bar, 10 μm. **(b)** Quantification of nuclear shape index in control and mechanically squeezed cells at the indicated time points (n=80). Nuclear perimeter and projected area were assessed using Image J software based on the fluorescent images. Nuclear shape index is defined as $4\pi \times A/C^2$, where A is the projected area of the nucleus and C is the perimeter of the nucleus. Statistical significance was determined at each time point by a two-tailed, unpaired t-test. All squeezing groups were compared with the Ctrl (200-μm) group. In b, box plots show the ends at the quartiles, the mean as a horizontal line in the box, and the whiskers represent the SD.

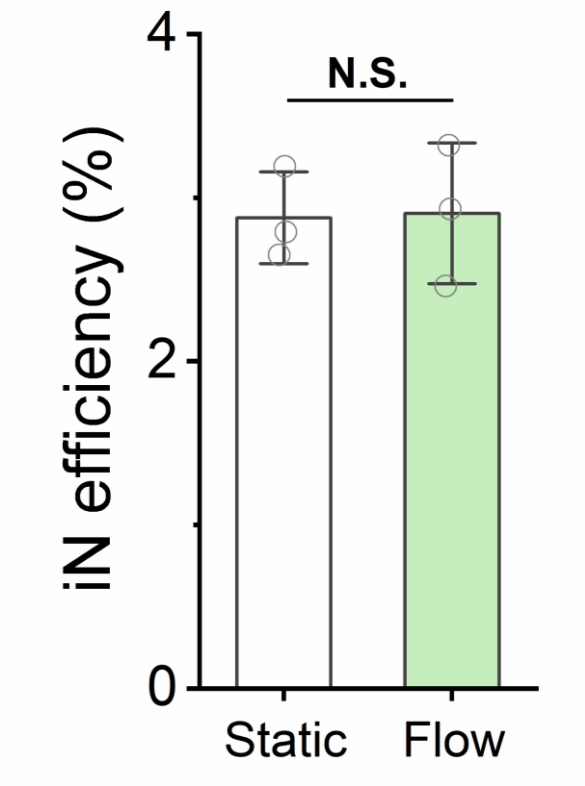

Supplementary Figure 9. Effect of flow on iN reprogramming. Reprogramming efficiency of BAM-transduced fibroblasts at day 7. For static conditions, cells were seeded on glass slides without being introduced into microchannels, whereas under flow conditions, cells were seeded onto glass slides after passing through 200-μm channels. At day 7, the cells were fixed and stained for Tubb3 by using Tuj1 antibody, followed by immunofluorescence microscopy to quantify $Tuj1^+$ iN cells. The reprogramming efficiency was determined based on Tuj1 staining (n=3). Statistical significance was determined by a two-tailed, unpaired t-test (NS: not significant). The data represent the mean ± SD.

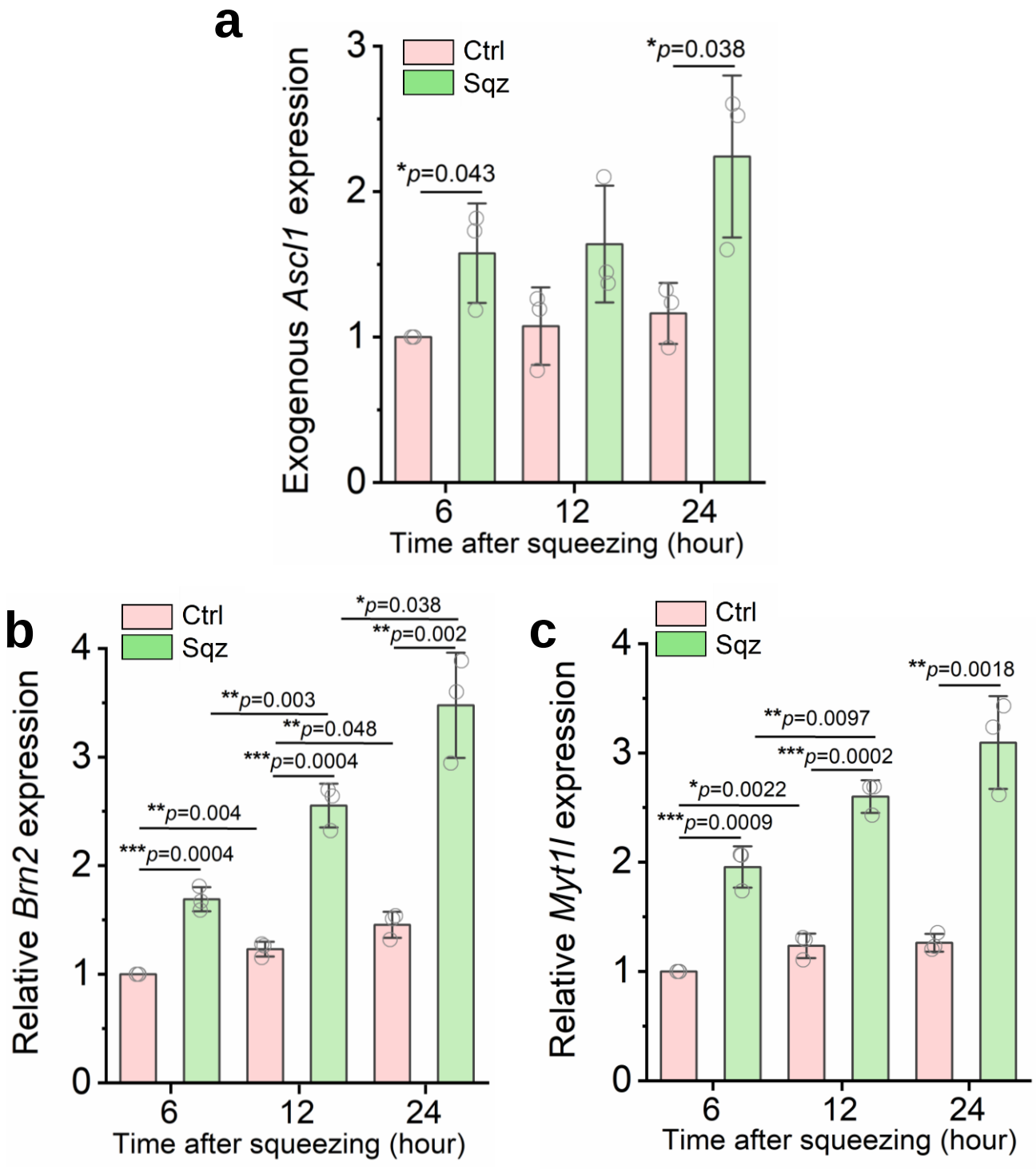

Supplementary Figure 10. Effect of mechanical squeezing on neuronal gene expression. At 6, 12 and 24 hours after BAM-transduced fibroblasts passed through 200-μm (Ctrl) or 7-μm (Sqz) microchannels, samples were collected, and RNA was isolated for PCR analysis. Relative gene expression of exogenous *Ascl1* **(a)**, *Brn2* **(b)** and *Myt1l* **(c)** in mechanically deformed (Sqz) and control (Ctrl) cells, where gene expression was normalized to 18S (n=3). Statistical significance was determined by a one-way ANOVA and Tukey's multiple comparison test. All squeezing (Sqz) groups were compared with the control (Ctrl) group. The data represent the mean ± SD.

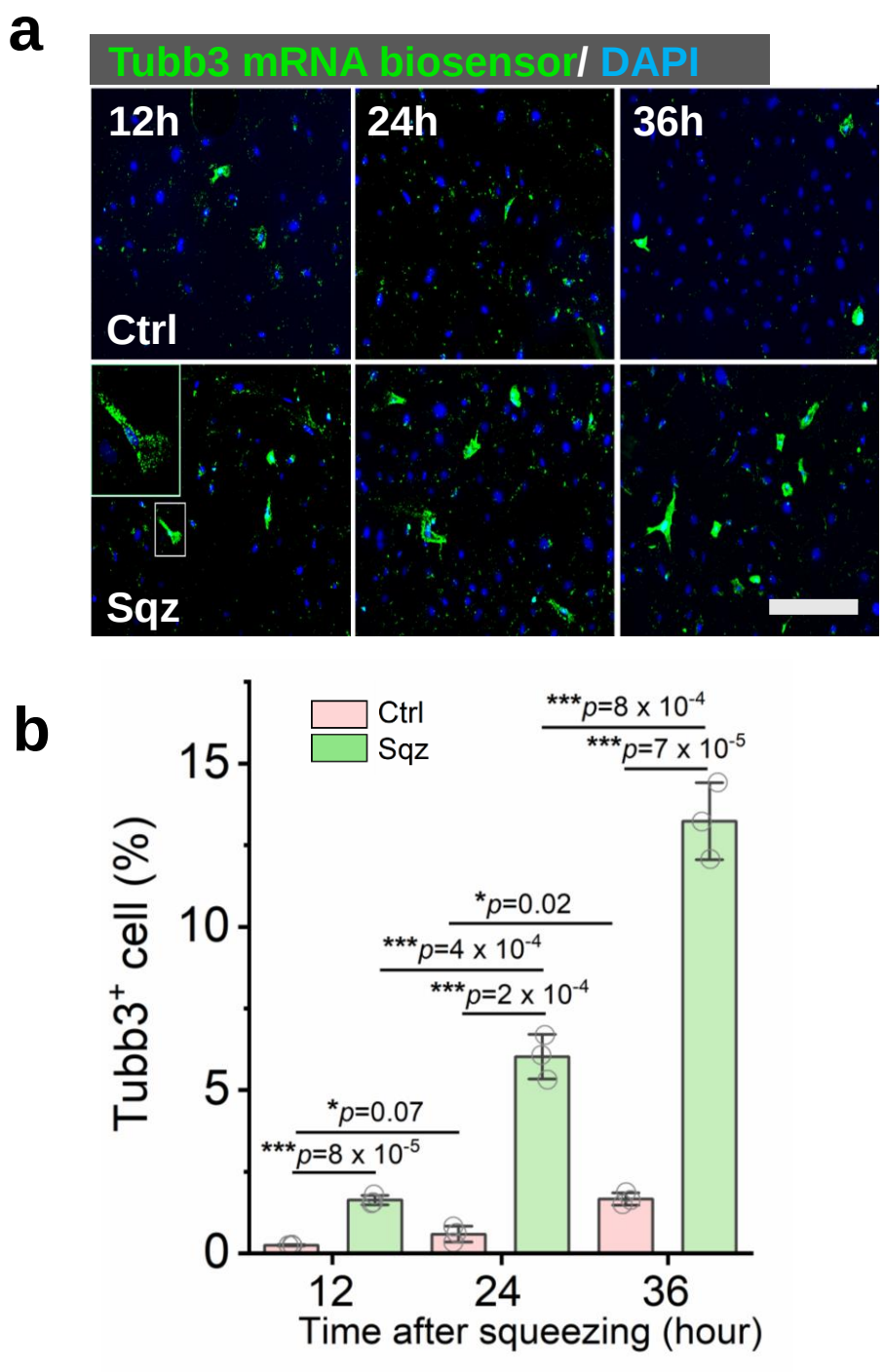

Supplementary Figure 11. Nuclear deformation promoted Tubb3 gene expression. At 12, 24 and 36 hours after BAM-transduced fibroblasts passed through 200-μm (Ctrl) or 7-μm (Sqz) microchannels, Tubb3 mRNA biosensor was added into the culture medium and incubated for 4 hours. The samples were washed 3 times by PBS, and images were taken by immunofluorescence microscopy. **(a)** Immunofluorescent images show Tubb3 mRNA expression in the cells of the control (Ctrl) and squeezed (Sqz) groups at the indicated time points after mechanical squeezing. Scale bar, 100 μm. **(b)** Quantification of the percentage of *Tubb3*$^{+}$ cells at the indicated time points (n=3). Statistical significance was determined by a one-way ANOVA and Tukey's multiple comparison test. All squeezing (Sqz) groups were compared with the control (Ctrl) group. The data represent the mean ± SD.

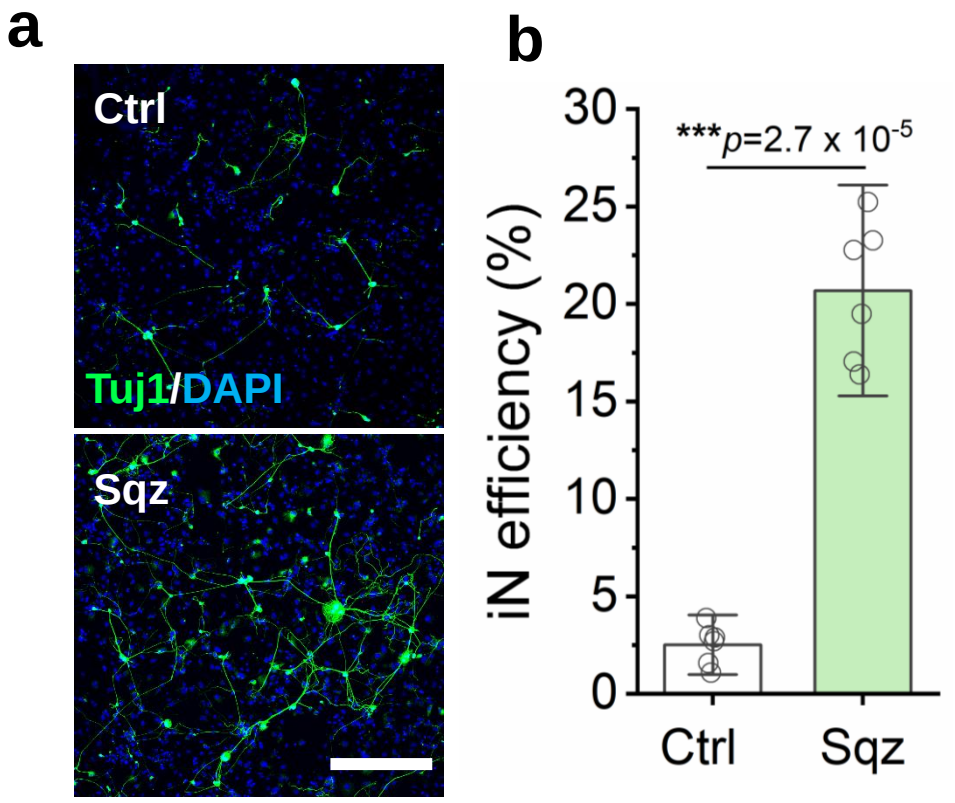

Supplementary Figure 12. Nuclear deformation enhanced iN reprogramming. BAM-transduced mouse fibroblasts were squeezed through 7-μm channels (Sqz) or 200-μm channels (Ctrl), seeded on fibronectin-coated surfaces, and cultured for 2 weeks. At day 14, the cells were fixed and stained for Tubb3 by using a Tuj1 antibody, followed by immunofluorescence microscopy to quantify Tuj1$^+$ iN cells. **(a)** Immunofluorescent images of Tuj1$^+$ iN cells on day 14. Scale bar, 200 μm. **(b)** Reprogramming efficiency of BAM-transduced fibroblasts in the control (Ctrl) and squeezed (Sqz) groups at day 14 (n=6). Statistical significance was determined by a two-tailed, unpaired t-test where the squeezed (Sqz) group was compared with the control (Ctrl) group. The data represent the mean ± SD.

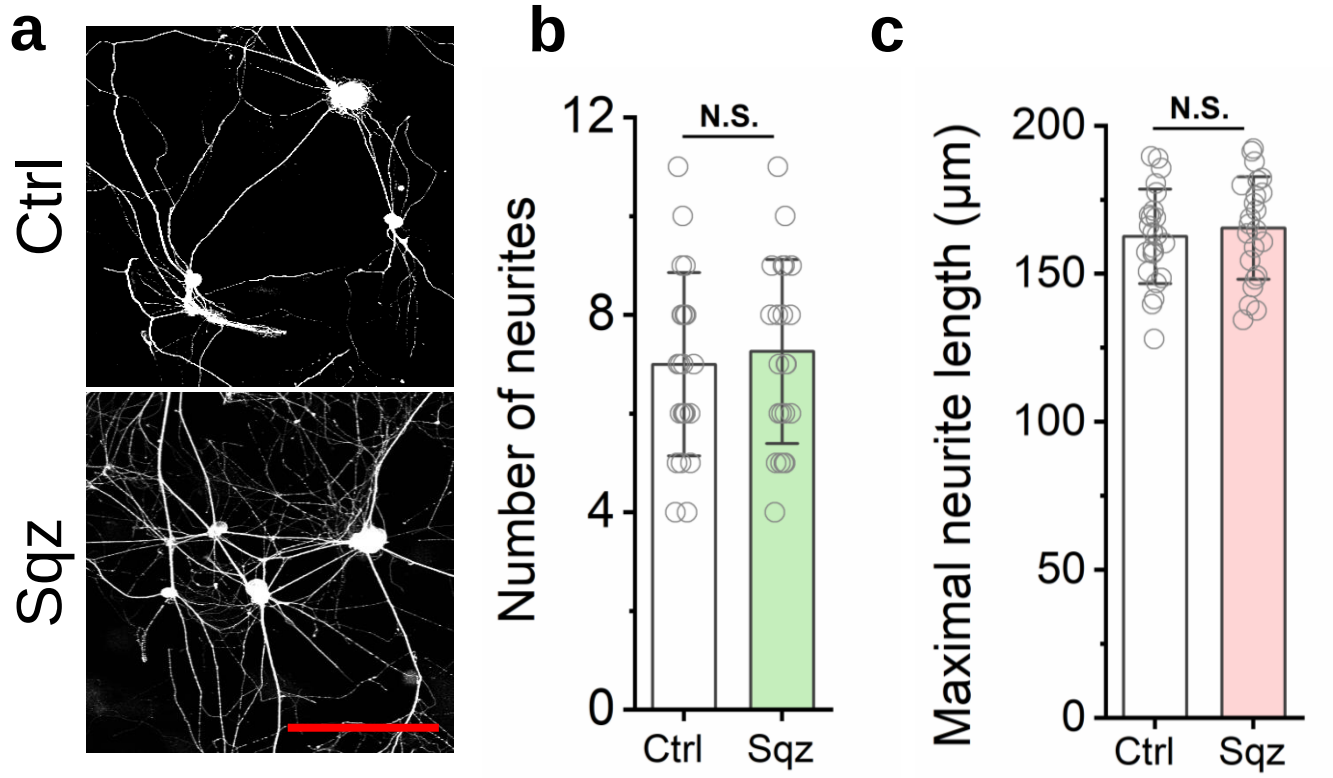

Supplementary Figure 13. Effect of nuclear deformation on neuronal morphology. BAM-transduced mouse fibroblasts were squeezed through 7-μm channels (Sqz) or 200-μm channels (Ctrl), seeded on fibronectin-coated surfaces, and cultured for 4 weeks. **(a)** Representative immunofluorescent images of Tuj1 staining showing the morphology of induced neurons. Scale bar, 100 μm. **(b)** Quantification of the number of neurites of each neuronal cell based on immunofluorescent images (n=20 cells). Statistical significance was determined by a two-tailed, unpaired t-test (NS: not significant), where squeezed (Sqz) group was compared with the control (Ctrl) group. **(c)** Quantification of the maximal neurite length of a neuronal cell based on immunofluorescent images (n= 20 cells). Statistical significance was determined by a two-tailed, unpaired t-test (NS: not significant), where squeezed (Sqz) group was compared with the control (Ctrl) group. The data represent the mean ± SD.

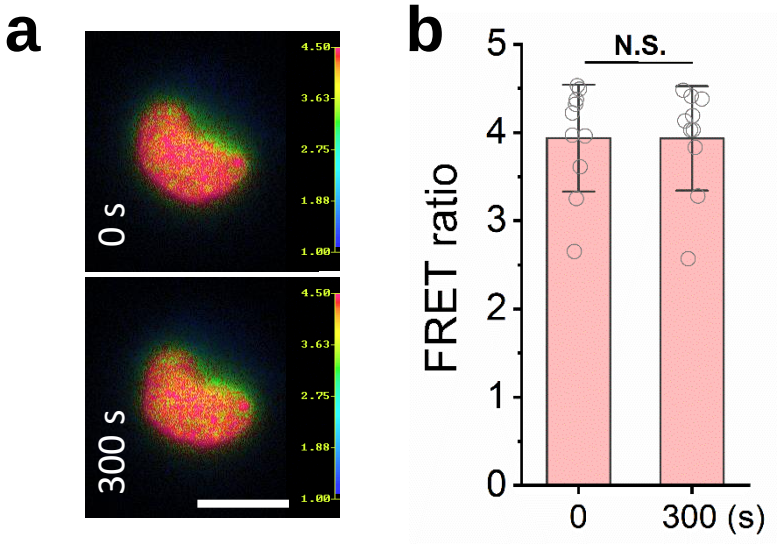

Supplementary Figure 14. Large microchannels did not alter H3K9me3 levels as detected by a FRET sensor. (a) Live cell imaging was performed to monitor FRET signal changes in H3K9me3 during cell deformation induced by 200-μm microchannels. Images were collected at 0 and 300 seconds as H3K9me3 FRET sensor-transduced fibroblasts passed through a 200-μm microchannel. Red color indicates higher level of H3K9me3, and green indicates lower FRET signal. Scale bar, 10 μm. **(b)** Quantification of H3K9me3 FRET signal at the indicated time points (n=10 cells). Statistical significance was determined by a two-tailed, unpaired t-test (NS: not significant). The data represent the mean ± SD.

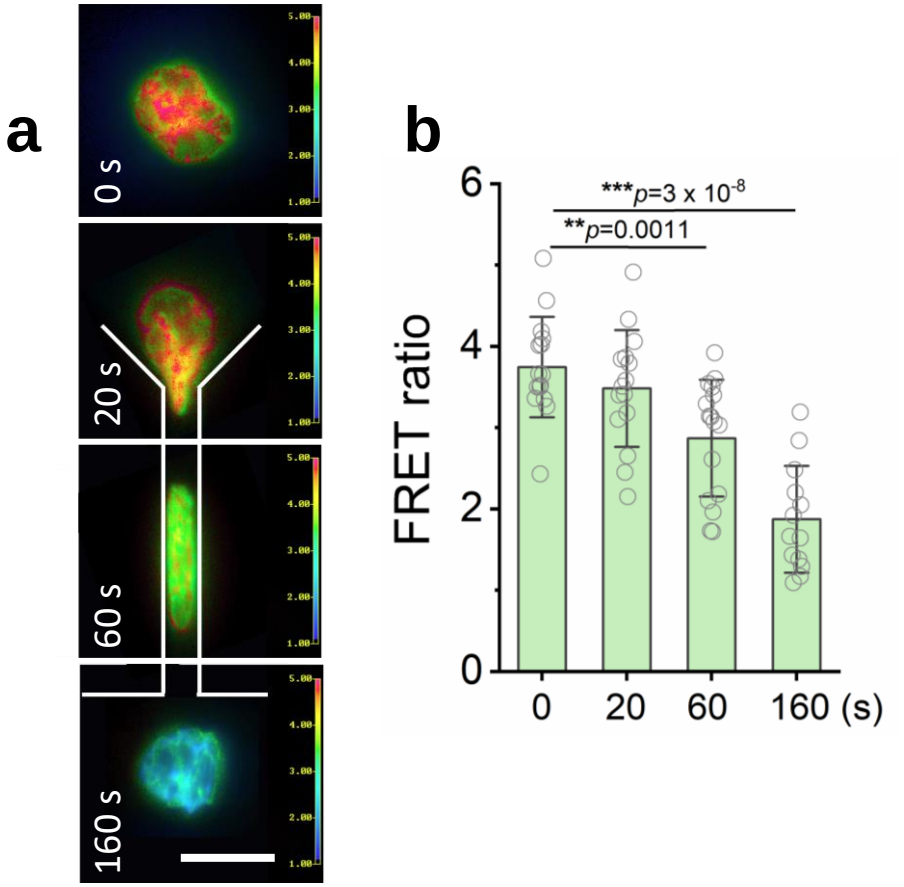

Supplementary Figure 15. Cell nucleus deformation in microchannel decreased H3K9me3 as detected by a FRET sensor. (a) Live cell imaging was performed to monitor FRET signal changes in H3K9me3 during cell deformation induced by a 7-μm microchannel. Images were captured at 0, 20, 60 and 160 seconds as H3K9me3 FRET sensor-transduced fibroblasts passed through a 7-μm microchannel. Red color indicates higher level of H3K9me3, and green indicates lower FRET signal. Scale bar, 10 μm. **(b)** H3K9me3 FRET signal was quantified at different time points (n=16 cells). Statistical significance was determined by a one-way ANOVA and Tukey's multiple comparison test where FRET signal ratio values were compared with the FRET signal ratio at 0 seconds. The data represent the mean ± SD.

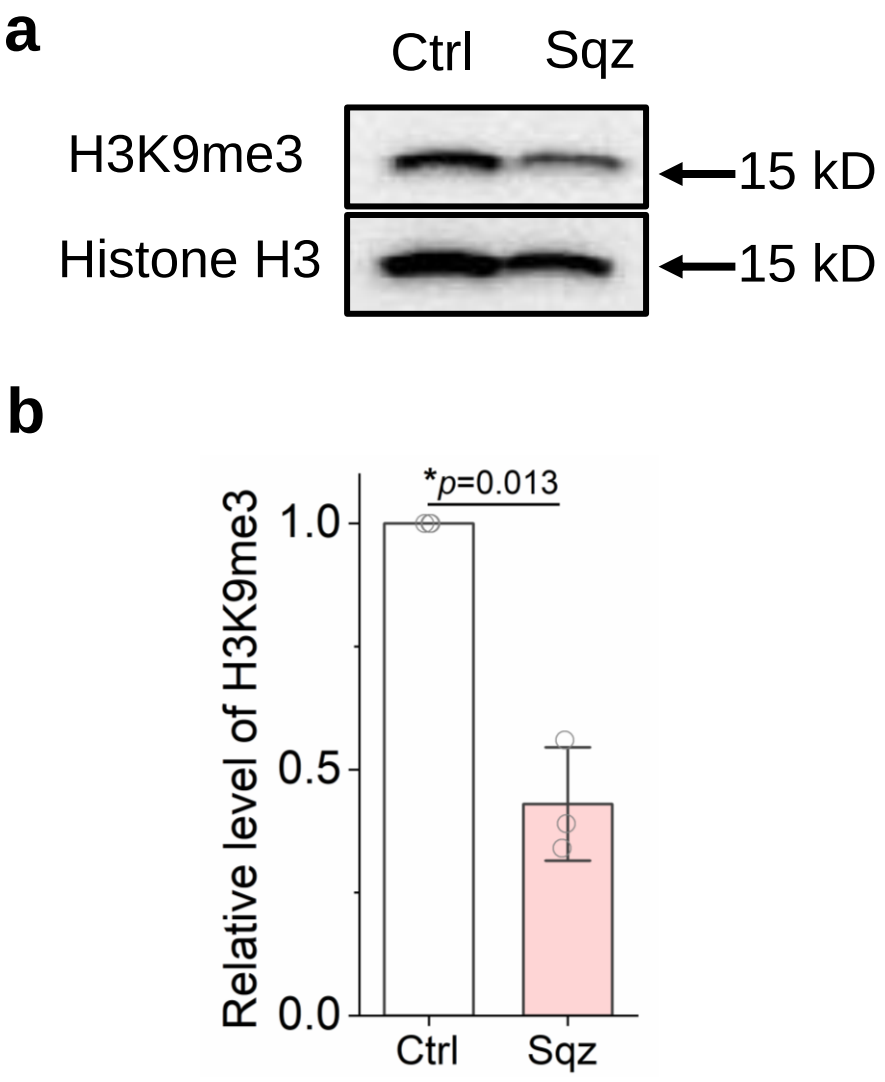

Supplementary Figure 16. Microchannel-induced nuclear deformation decreased global H3K9me3. (a) Total histone extracts were isolated from BAM-transduced fibroblasts using the Histone Extraction Kit (Abcam, ab221031, USA) at 3 hours after the cells passed through the microchannels. Western blotting was used to examine the levels of H3K9me3 and histone H3. Control (Ctrl): cells passing through 200-μm channels. Squeezed (Sqz): cells passing through 7-μm microchannels. **(b)** Quantification of H3K9me3 from Western blots (n=3). Statistical significance was determined by a two-tailed, unpaired t-test where squeezed (Sqz) group was compared with the control (Ctrl) group. The data represent the mean ± SD.

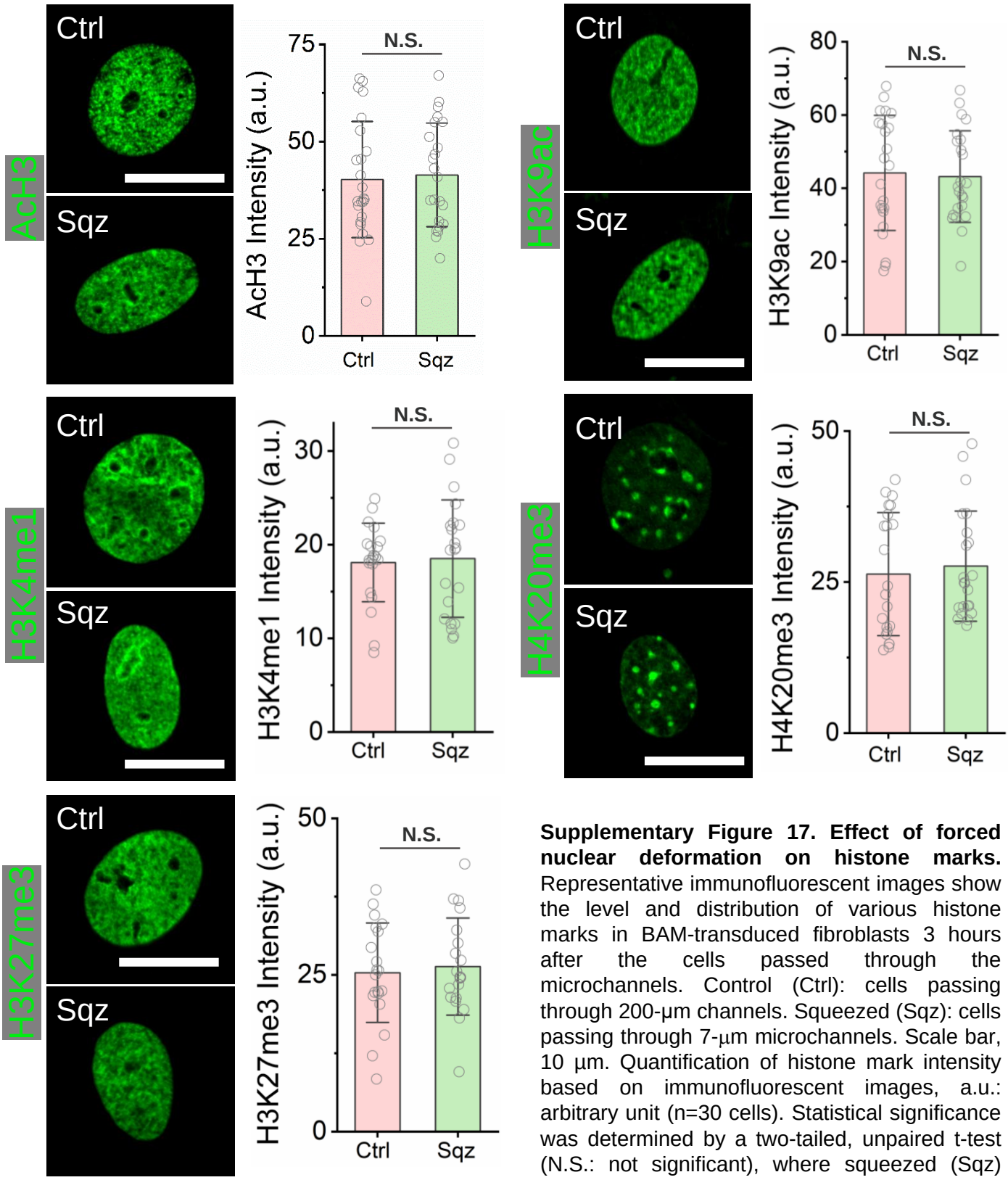

Supplementary Figure 17. Effect of forced nuclear deformation on histone marks. Representative immunofluorescent images show the level and distribution of various histone marks in BAM-transduced fibroblasts 3 hours after the cells passed through the microchannels. Control (Ctrl): cells passing through 200-μm channels. Squeezed (Sqz): cells passing through 7-μm microchannels. Scale bar, 10 μm. Quantification of histone mark intensity based on immunofluorescent images, a.u.: arbitrary unit (n=30 cells). Statistical significance was determined by a two-tailed, unpaired t-test (N.S.: not significant), where squeezed (Sqz) group was compared with the control (Ctrl) group. The data represent the mean ± SD.

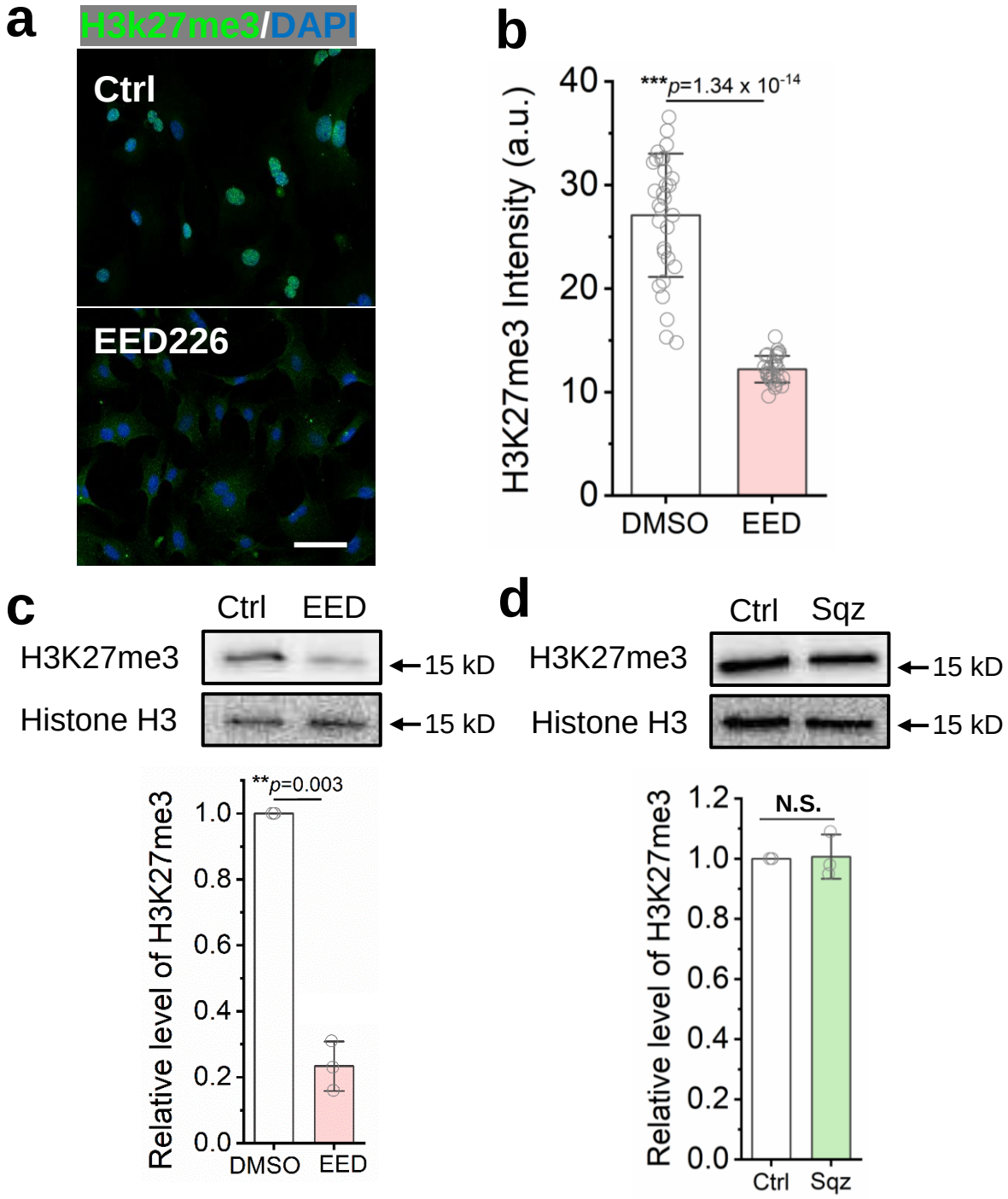

Supplementary Figure 18. Microchannel-induced nuclear deformation did not alter H3K27me3. Fibroblasts were seeded on fibronectin-coated cover glass, and treated with H3K27me3 inhibitor EED226 (EED, 10 μM) or DMSO (solvent control) for 24 hours. **(a)** Representative immunofluorescent images show H2K27me3 staining in fibroblasts treated with EED or DMSO for 24 hours. Scale bar, 50 μm. **(b)** Quantification of H3K27me3 intensity based on immunofluorescent images (n=30 cells). Statistical significance was determined by a two-tailed, unpaired t-test. **(c)** Western blotting was used to examine the levels of H3K27me3 and histone H3 in fibroblasts treated with EED or DMSO for 24 hours. Bar graph shows the quantification of H3K27me3 from Western blots (n=3). Statistical significance was determined by a two-tailed, unpaired t-test (N.S.: not significant), where EDD226 treated group (EDD) was compared with the control group (DMSO). **(d)** Western blotting was used to examine the levels of H3K27me3 and histone H3 in BAM-transduced fibroblasts at 3 hours after the cells passed through 200-μm (Ctrl) or 7-μm microchannels (Sqz). Bar graph shows the quantification of H3K27me3 from Western blots (n=3). Statistical significance was determined by a two-tailed, unpaired t-test (NS: not significant), where squeezed (Sqz) group was compared with the control (Ctrl) group. The data represent the mean ± SD.

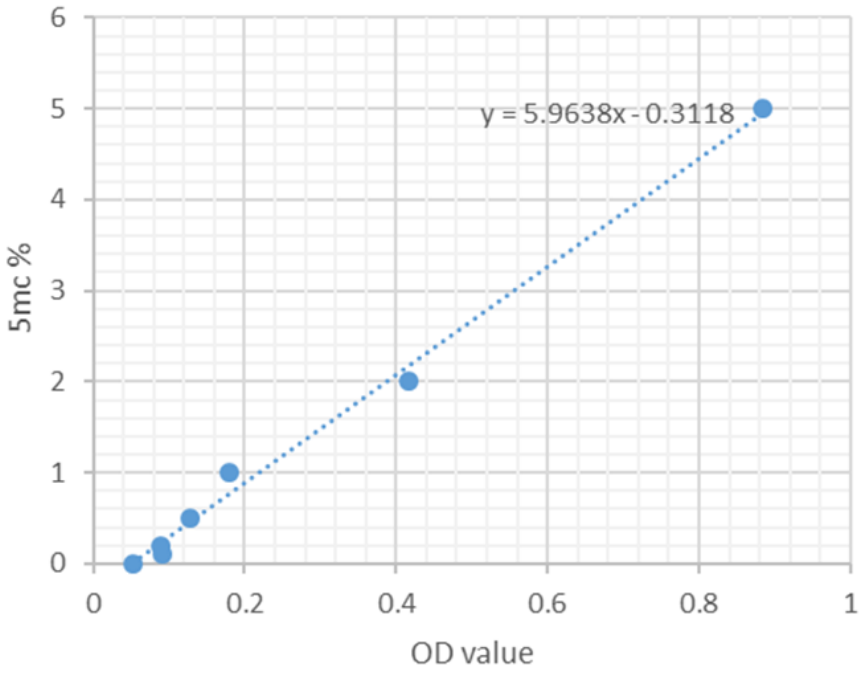

Supplementary Figure 19. 5-mC standard curve. The 5-mC standard sample was diluted to 0.1% to 5% (1 µg/ml to 50 µg/ml) according to the manufacturer's instructions for the MethylFlashTM Global DNA Methylation (5-mC) ELISA Easy Kit (Epigentek, P-1030), and bonded into the assay wells and incubated with 5-mC detection complex solution for 60 minutes. The color developer solution was added into assay wells, and absorbance was detected by using a plate reader (Infinite 200Pro, 30050303) at 450 nm. Based on the average OD value on the X-axis and the known 5-mC percentage at each point on the Y-axis, we generated the standard curve between 5-mC % and OD value. This standard curve was used to calculate the 5-mC level in cells.

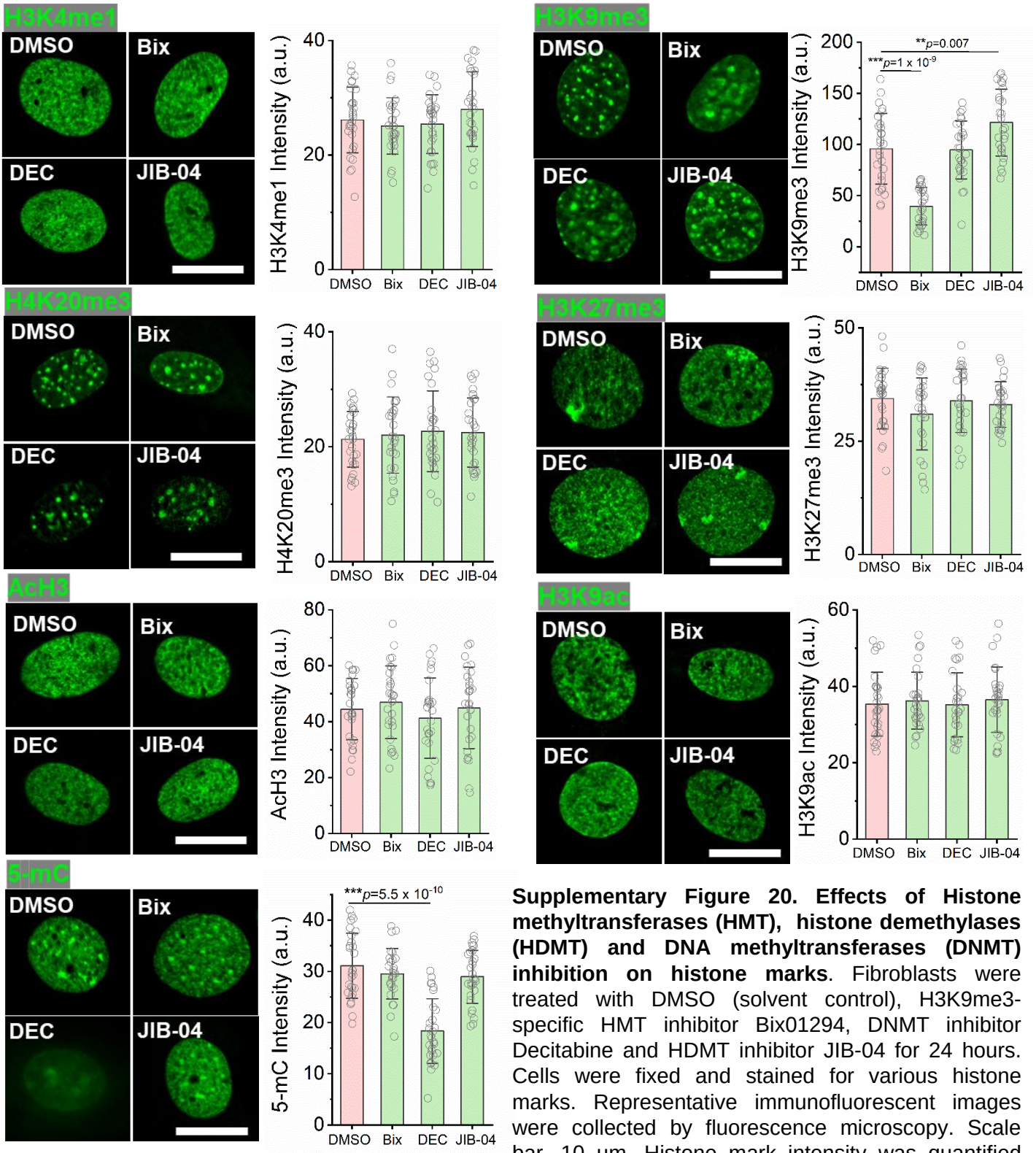

Supplementary Figure 20. Effects of Histone methyltransferases (HMT), histone demethylases (HDMT) and DNA methyltransferases (DNMT) inhibition on histone marks. Fibroblasts were treated with DMSO (solvent control), H3K9me3-specific HMT inhibitor Bix01294, DNMT inhibitor Decitabine and HDMT inhibitor JIB-04 for 24 hours. Cells were fixed and stained for various histone marks. Representative immunofluorescent images were collected by fluorescence microscopy. Scale bar, 10 µm. Histone mark intensity was quantified based on immunofluorescent images, a.u.: arbitrary unit (n=30 cells). Significance was determined by a one-way ANOVA and Tukey's multiple comparison test, where chemical-treated groups were compared with the DMSO group. The data represent the mean ± SD.

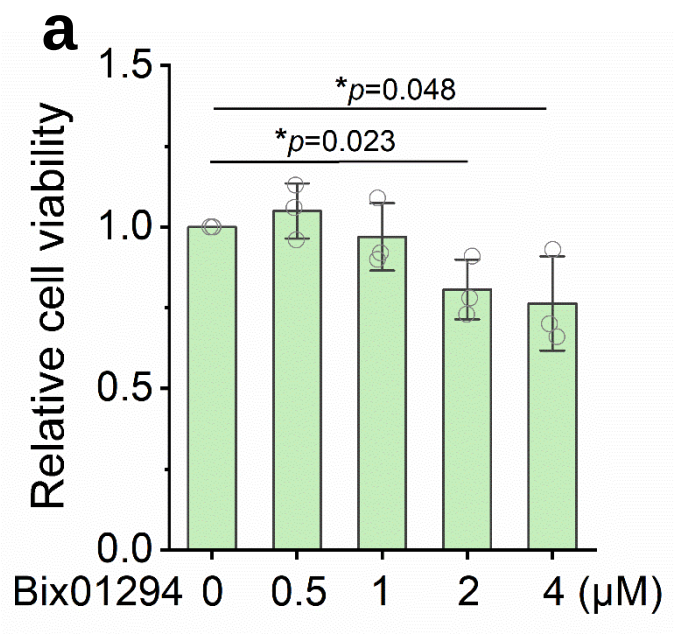

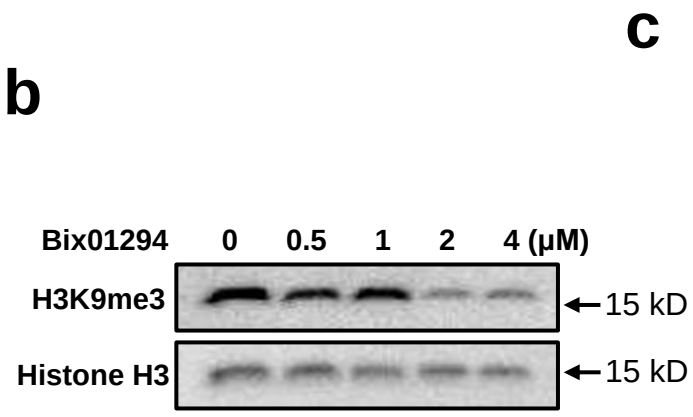

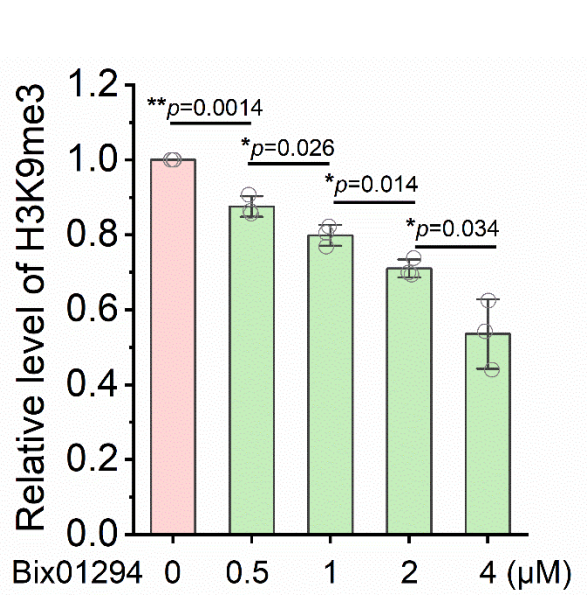

Supplementary Figure 21. Effects of histone methyltransferase (HMT) inhibition on cell viability and H3K9me3. (a) Fibroblasts were treated with HMT inhibitor Bix01294 at various concentrations for 24 hours, and cell viability was determined by using the PrestoBlue® Cell Viability assay (n=3). Cell viability was normalized with the solvent control (the viability of cells treated by DMSO). Statistical significance was determined by a one-way ANOVA and Tukey's multiple comparison test. **(b)** Western blotting analysis of H3K9me3 in fibroblasts that were treated with HMT inhibitor Bix01294 at various concentrations for 24 hours. Fibroblasts treated with DMSO (solvent control) served as a control. **(c)** Quantification of H3K9me3 from blots (n=3). Statistical significance was determined by a one-way ANOVA and Tukey's multiple comparison test, where all Bix0129-treated groups were compared with the control (DMSO) group. The data represent the mean ± SD.

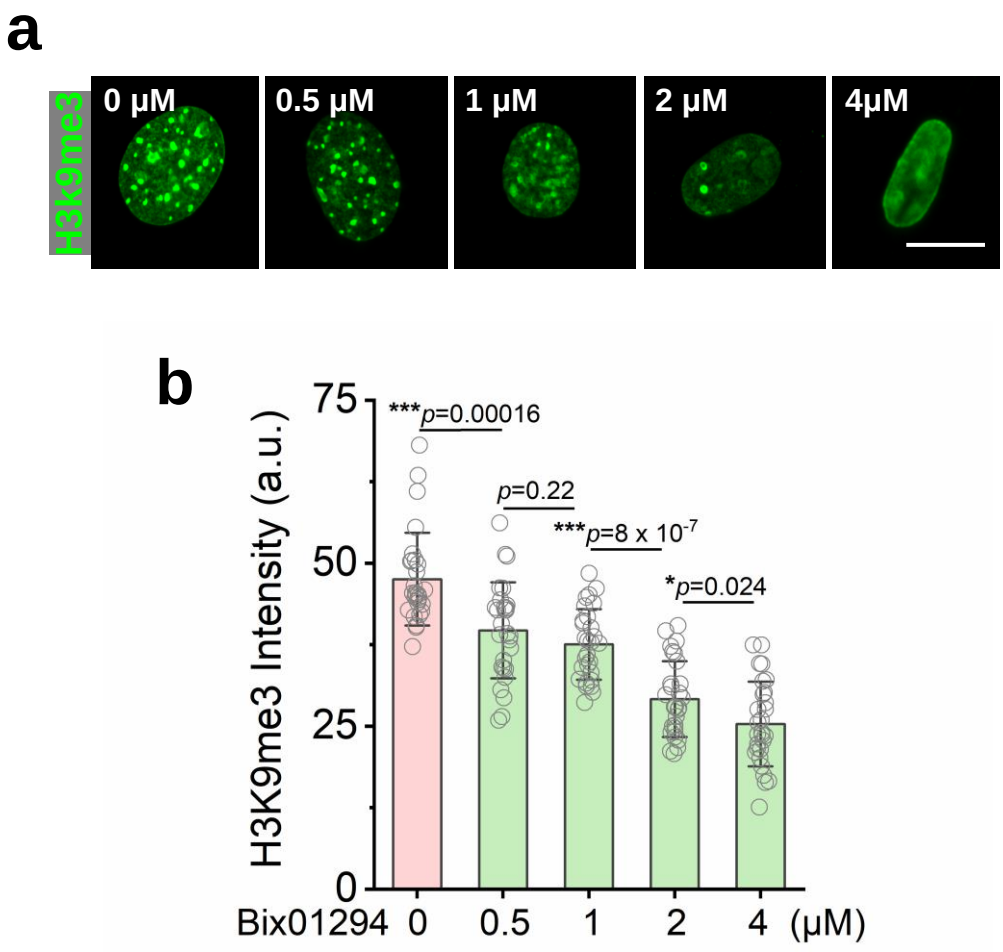

Supplementary Figure 22. Characterization of histone methyltransferase (HMT) inhibition. (a) Representative immunofluorescent images show the level and distribution of H3K9me3 in BAM-transduced fibroblasts pre-treated with different doses of HMT inhibitor, Bix01294, for 24 hours. Scale bar, 10 μm. **(b)** Quantification of H3K9me3 intensity from immunofluorescent images (n=30 cells). Statistical significance was determined by a one-way ANOVA and Tukey's multiple comparison test, where all Bix0129-treated groups were compared with the control (DMSO) group. The data represent the mean ± SD.

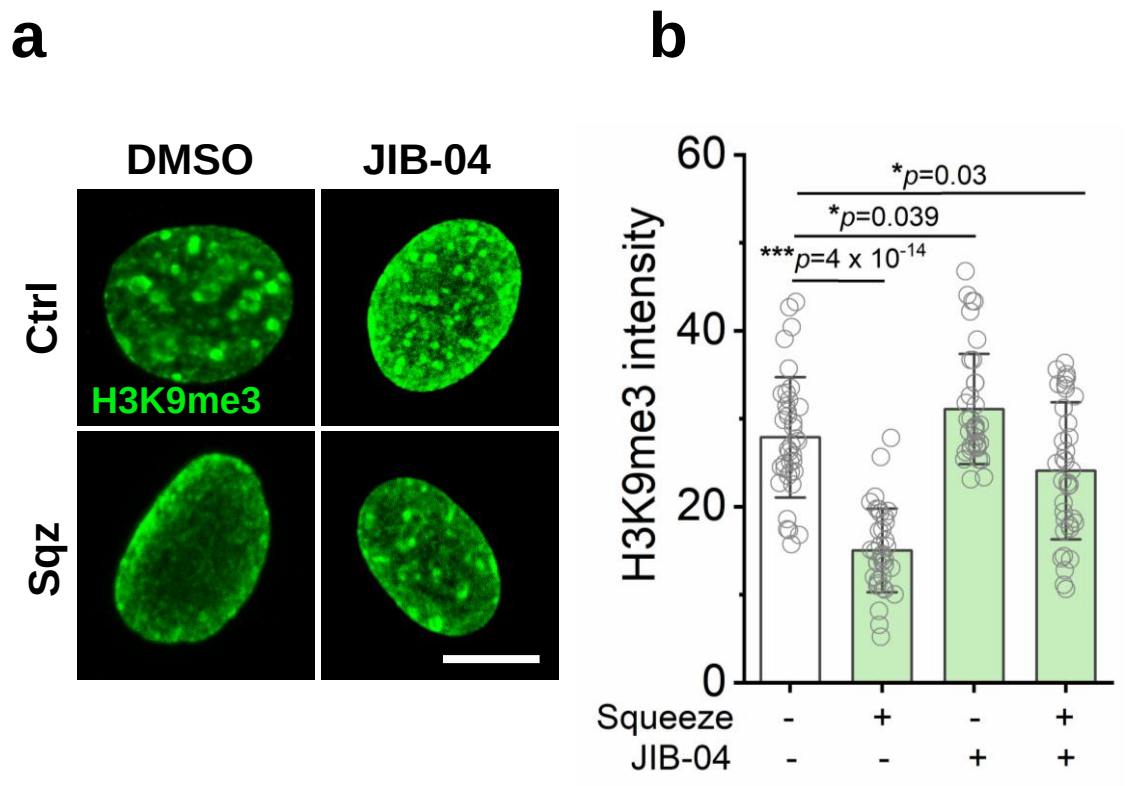

Supplementary Figure 23. Effect of histone demethylase inhibition on mechanical squeezing-induced H3K9me3 suppression based on immunofluorescence imaging. Mouse fibroblasts were pretreated with histone demethylase inhibitor JIB-04 (100 nM) for 24 hours before passing through the microchannels, and the effects on H3K9me3 were examined. **(a)** Representative immunofluorescent images show the level and distribution of H3K9me3 in fibroblasts 3 hours after the cells passed through the microchannels. Control (Ctrl): cells passing through 200-μm channels. Squeezed (Sqz): cells passing through 7-μm microchannels. Scale bar, 5 μm. **(b)** Histone mark intensity was quantified based on immunofluorescent images (n=30 cells). Statistical significance was determined by a one-way ANOVA and Tukey's multiple comparison test, where all JIB-04-treated groups and squeezed (Sqz) groups were compared with the control (DMSO) group. The data represent the mean ± SD.

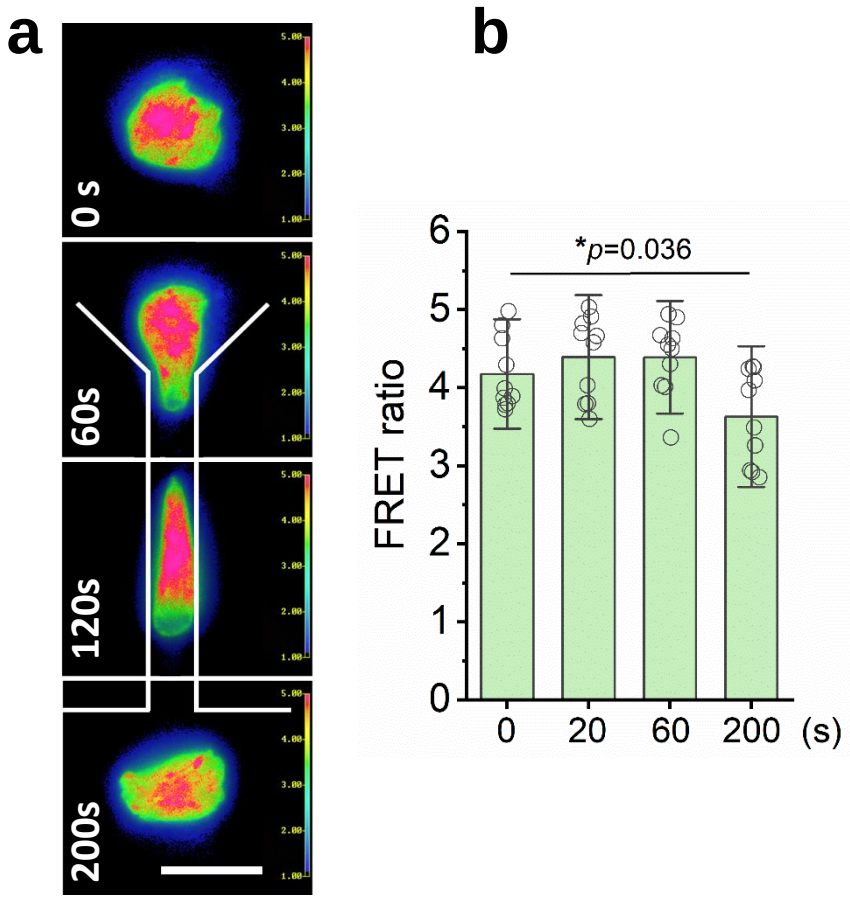

Supplementary Figure 24. Effect of histone demethylase inhibition on mechanical squeezing-induced H3K9me3 suppression based on FRET imaging. H3K9me3 FRET sensor-transduced mouse fibroblasts were pretreated with histone demethylase inhibitor JIB-04 (100 nM) for 24 hours before passing through the microchannels, and the effects on H3K9me3 were examined. (a) Mouse fibroblasts expressing the H3K9me3 FRET sensor were passed through 7-mm microchannels and live cell imaging was performed to monitor changes in H3K9me3 during cell deformation induced by a 7-μm microchannel. Red color indicates higher level of H3K9me3, and green indicates lower FRET signal. Scale bar, 10 μm. (b) H3K9me3 FRET signal was quantified at different time points (n=10 cells). Statistical significance was determined by a one-way ANOVA and Tukey's multiple comparison test, where the FRET signal ratio at 20, 60 and 200 seconds was compared with the FRET signal ratio at 0 seconds. The data represent the mean ± SD.

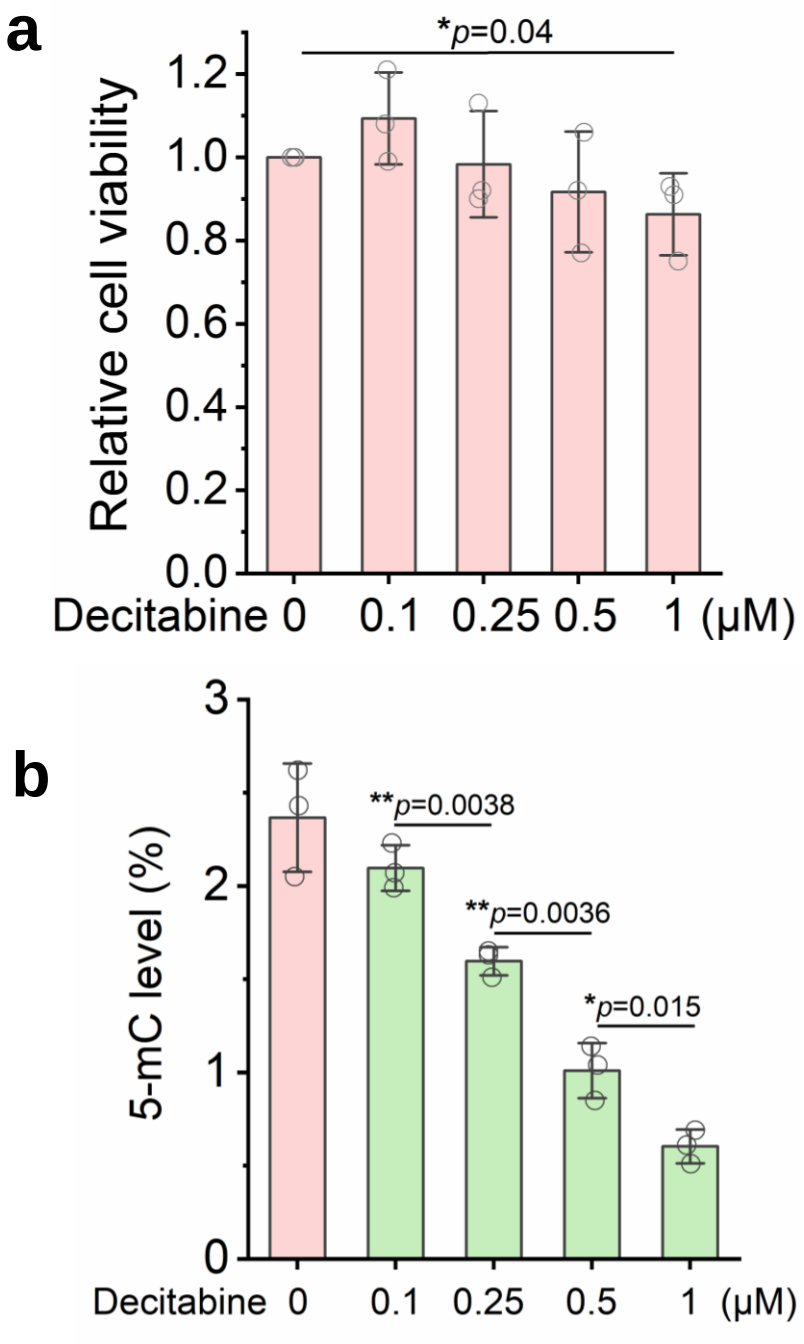

Supplementary Figure 25. Effect of DNMT inhibition on cell viability and DNA methylation. (a) Fibroblasts were treated with DNMT inhibitor Decitabine at various concentrations for 24 hours, followed by a cell viability assay, where cell viability was normalized with the solvent control (the viability of cells treated by DMSO) (n=3). Statistical significance was determined by a one-way ANOVA and Tukey's multiple comparison test, where all Decitabine-treated groups were compared with the control (DMSO) group. **(b)** Quantification of 5-mC level in fibroblasts treated with Decitabine at various concentrations for 24 hours as determined by using the MethylFlashTM Global DNA Methylation (5-mC) ELISA Easy Kit (n=3). Statistical significance was determined by a one-way ANOVA and Tukey's multiple comparison test. All Decitabine-treated groups were compared with the control (DMSO) group. The data represent the mean ± SD.

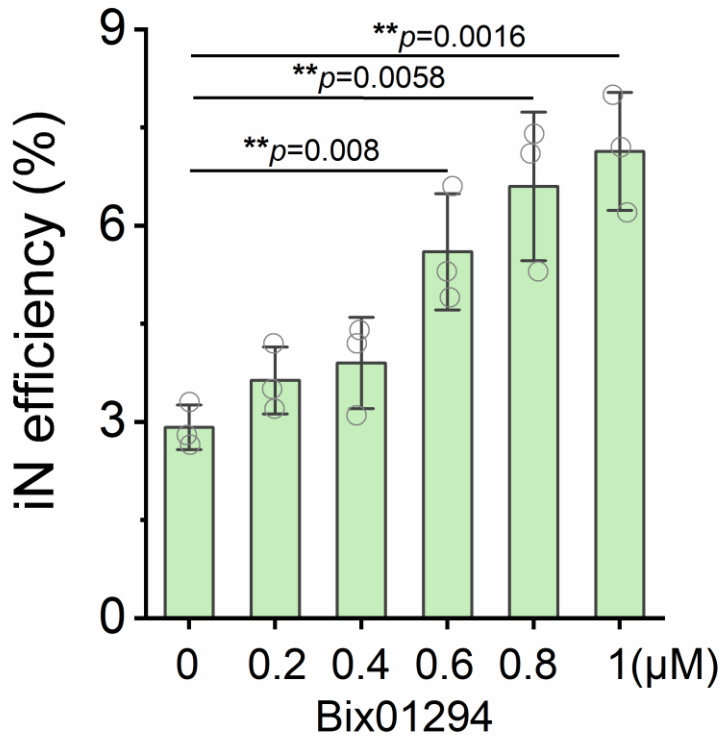

Supplementary Figure 26. Effect of HMT inhibition on iN reprogramming efficiency. Reprogramming efficiency of BAM-transduced fibroblasts that were pretreated with Bix01294 (0.2-1 μM) for 24 hours before adding Dox where cells treated with DMSO were used as a control. At day 7, the cells were fixed and stained for Tubb3 by using a Tuj1 antibody, followed by immunofluorescence microscopy to quantify $Tuj1^{+}$ iN cells. The reprogramming efficiency was determined based on Tuj1 staining (n=3). Statistical significance was determined by a one-way ANOVA and Tukey's multiple comparison test. All Bix0194-treated groups were compared with the control (DMSO) group. The data represent the mean ± SD.

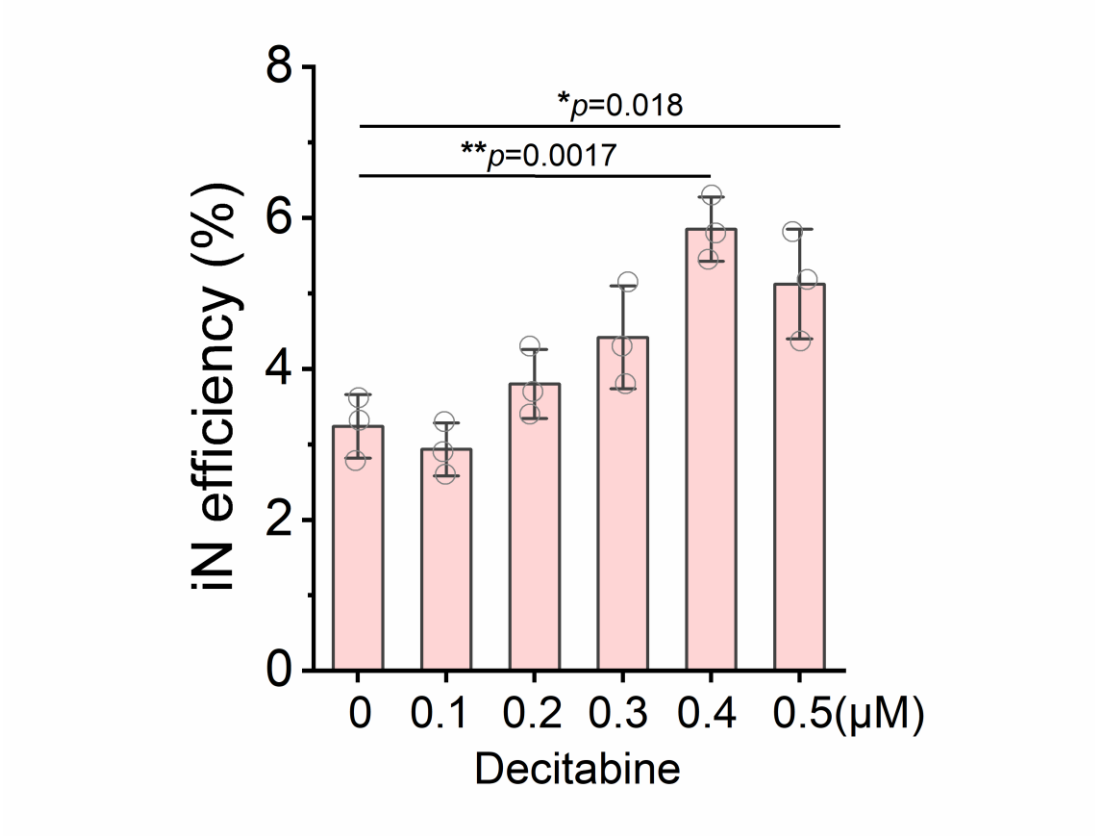

Supplementary Figure 27. Effect of DNMT inhibition on iN reprogramming efficiency. Reprogramming efficiency of BAM-transduced fibroblasts that were pretreated with Decitabine (0.1-0.5 μM) for 24 hours before adding Dox where cells treated with DMSO was used as a control. At day 7, the cells were fixed and stained for Tubb3 by using Tuj1 antibody, followed by immunofluorescence microscopy to quantify Tuj1^{+} iN cells. The reprogramming efficiency was determined based on Tuj1 staining (n=3). Statistical significance was determined by a one-way ANOVA and Tukey's multiple comparison test. All Decitabine-treated groups were compared with the control (DMSO) group. The data represent the mean ± SD.

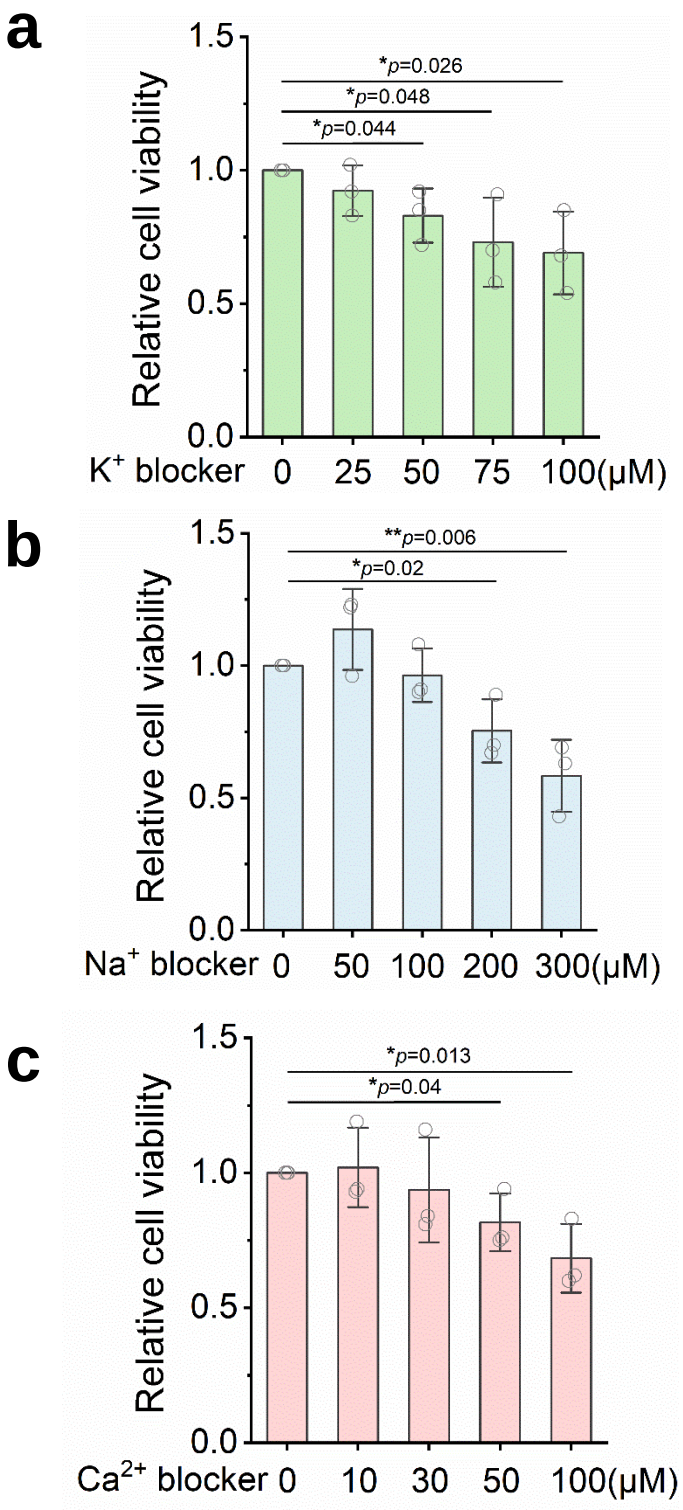

Supplementary Figure 28. Effect of ion channel inhibition on cell viability. Fibroblasts were treated with blockers of ion channels for potassium (quinine) (**a**), sodium (procainamide) (**b**), and calcium (amlodipine) (**c**), respectively, at the indicated concentrations for 12 hours before analyzing cell viability by using the PrestoBlue® Cell Viability Reagent (n=3). Cells treated with DMSO served as a control. Statistical significance was determined by a one-way ANOVA and Tukey's multiple comparison test. All ion channel blocker-treated groups were compared with the control (DMSO) group. The data represent the mean ± SD.

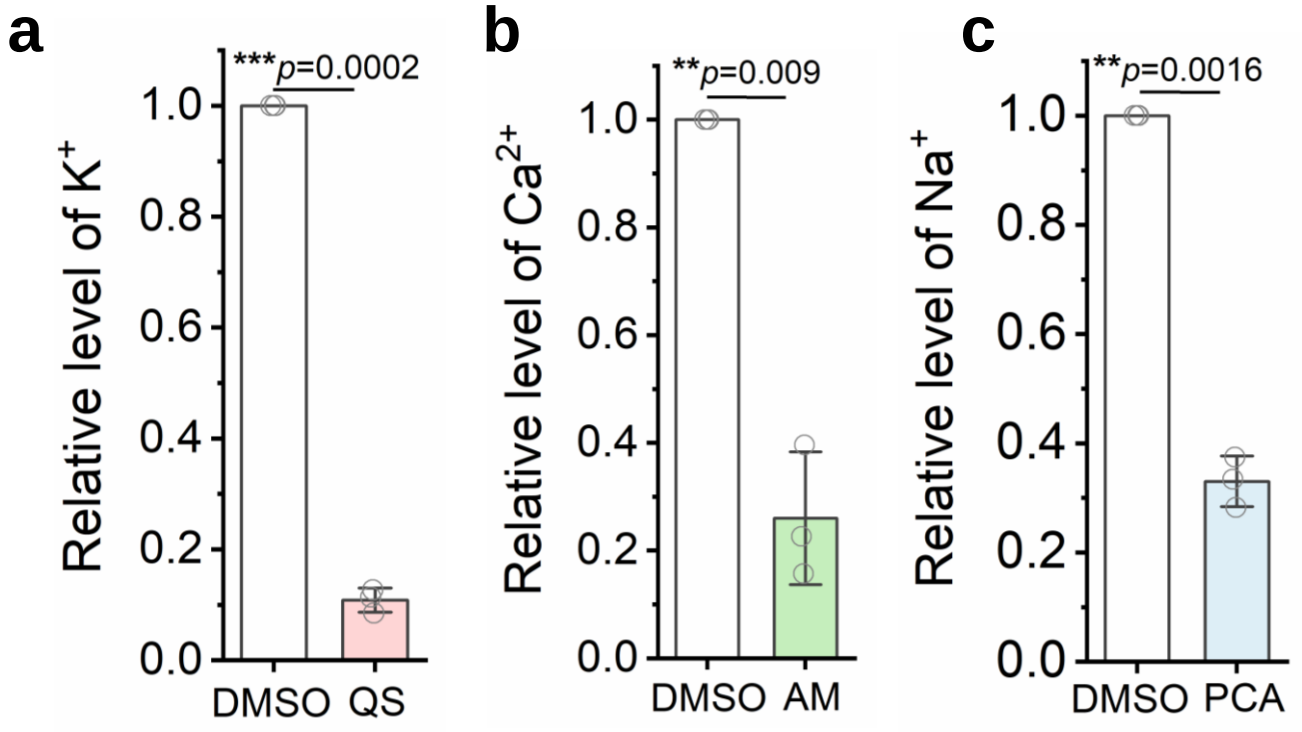

Supplementary Figure 29. Characterization of ion channel inhibition. Fibroblasts were treated with blockers of ion channels for potassium (quinine, QS, 25 μM) **(a)**, calcium (amlodipine, AM, 30 μM) **(b)**, and sodium (procainamide, PCA, 100 μM) **(c)**, respectively, for 12 hours before ion indicators were used to detect ion levels (n=3). Fluo-4 AM was used for calcium flux detection, Sodium Green™ Tetraacetate was used for sodium flux detection, and FluxOR™ Potassium Ion Channel Assay was used for potassium flux detection. Before measuring FluxOR™ II Green ion levels, cells were treated with stimulus buffers (10mM $CaCl_2$ and 10mM NaCl, respectively) for 30 minutes. The Potassium assay kit contains the Potassium Sulfate Stimulus Buffer (10 mM) for opening the ion channel. A plate-reader was utilized to acquire absorbance measurements. Cells treated with DMSO served as a control. Statistical significance was determined by a two-tailed, unpaired t-test. All ion channel blocker-treated groups were compared with the control (DMSO) group. The data represent the mean ± SD.

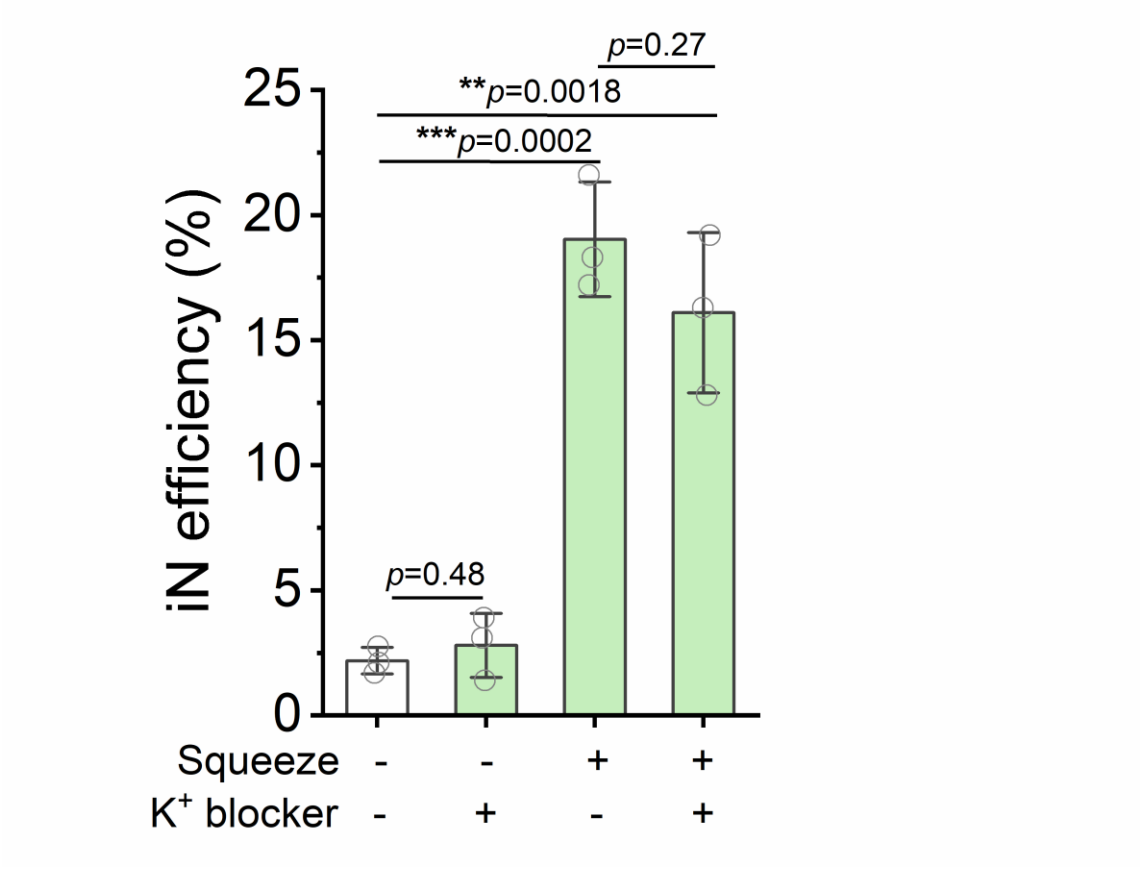

Supplementary Figure 30. Blocking potassium ion channels did not significantly affect microchannel-induced iN reprograming. BAM-transduced fibroblasts were pretreated with the potassium blocker Quinine (25 μM) for 12 hours before passing through 7-μm microchannels where cells passing through 200-μm channels were used as a control. . Quinine was only administered before squeezing to test its effect on squeezing-induced signaling, and was not used during the course of the reprogramming process. After cells passed through the microdevice, fibroblasts were seeded on fibronectin-coated glass slides and cultured in N2B27 medium for 7 days. At day 7, the cells were fixed and stained for Tubb3 by using a Tuj1 antibody, followed by immunofluorescence microscopy to quantify $Tuj1^+$ iN cells. The reprogramming efficiency was determined based on Tuj1 staining (n=6). Statistical significance was determined by a one-way ANOVA and Tukey's multiple comparison test, where all quinine-treated and squeezed groups were compared with the control group. The data represent the mean ± SD.

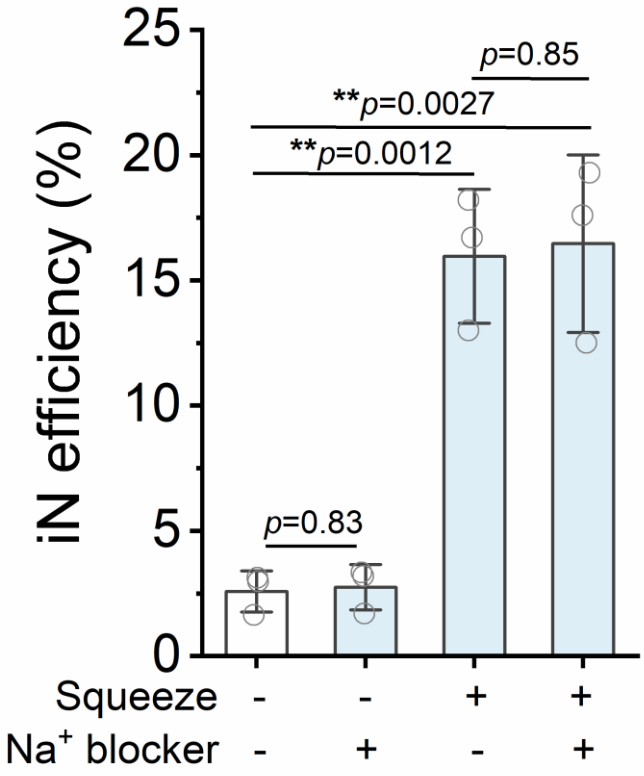

Supplementary Figure 31. Blocking sodium ion channels did not significantly affect microchannel-induced iN reprograming. BAM-transduced fibroblasts were pretreated with the sodium channel blocker Procainamide (100 μM) for 12 hours before passing through 7-μm microchannels where cells passing through 200-μm channels were used as a control. After cells passed through the microdevice, fibroblasts were seeded on fibronectin-coated glass slides and cultured in N2B27 medium for 7 days. At day 7, the cells were fixed and stained for Tubb3 by using a Tuj1 antibody, followed by immunofluorescence microscopy to quantify $Tuj1^+$ iN cells. The reprogramming efficiency was determined based on Tuj1 staining (n=6). Statistical significance was determined by a one-way ANOVA and Tukey's multiple comparison test, where all procainamide-treated and squeezed groups were compared with the control group. The data represent the mean ± SD.

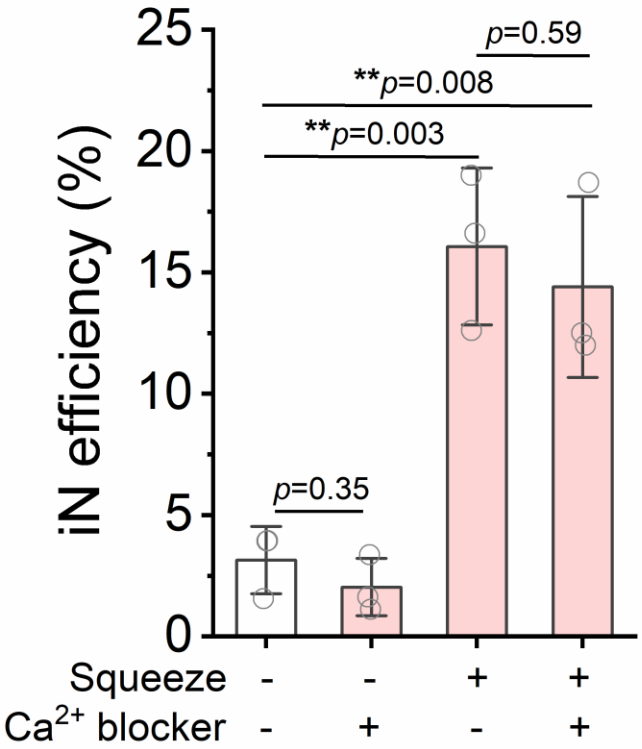

Supplementary Figure 32. Calcium ion channels did not regulate microchannel-induced iN reprograming. BAM-transduced fibroblasts were pretreated with the calcium channel blocker Amlodipine (30 μM) for 12 hours before passing through 7-μm microchannels where cells passing through 200-μm channels were used as a control. After cells passed through the microdevice, fibroblasts were seeded on fibronectin-coated glass slides and cultured in N2B27 medium for 7 days. At day 7, the cells were fixed and stained for Tubb3 by using a Tuj1 antibody, followed by immunofluorescence microscopy to quantify $Tuj1^+$ iN cells. The reprogramming efficiency was determined based on Tuj1 staining (n=6). Statistical significance was determined by a one-way ANOVA and Tukey's multiple comparison test, where all amlodipine-treated and squeezed groups were compared with the control group. The data represent the mean ± SD.

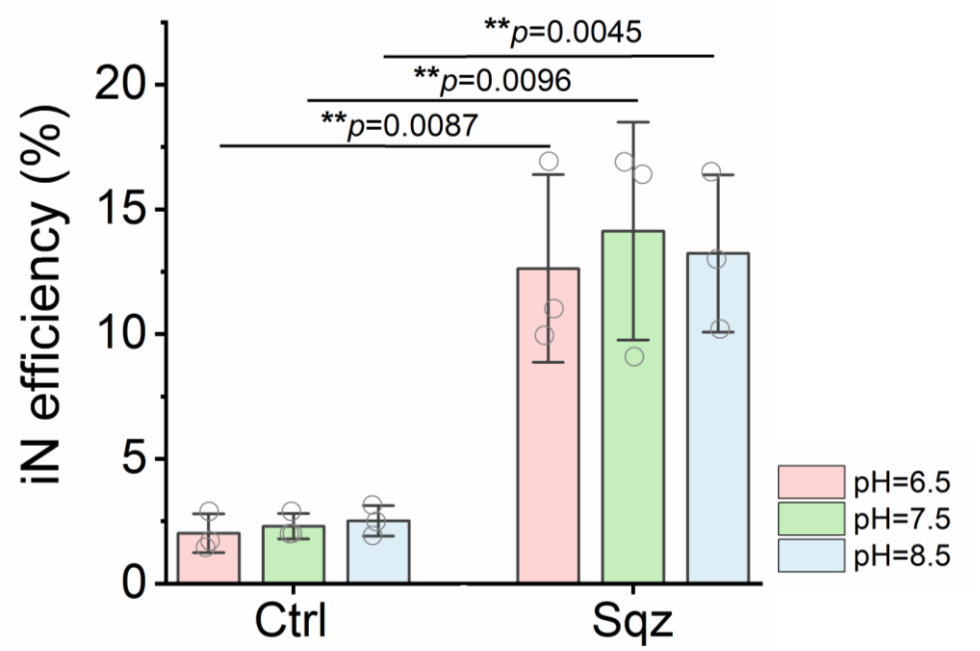

Supplementary Figure 33. Extracellular pH did not affect microchannel-induced iN reprograming. BAM-transduced fibroblasts were pretreated with culture media at different pH for 1 hour before passing through 7-μm microchannels. After cells passed through the microdevice, fibroblasts were seeded on fibronectin-coated glass slides and cultured in N2B27 medium for 7 days. At day 7, the cells were fixed and stained for Tubb3 by using a Tuj1 antibody, followed by immunofluorescence microscopy to quantify $Tuj1^{+}$ iN cells. The reprogramming efficiency was determined based on Tuj1 staining (n=3). Control (Ctrl): cells passing through 200-μm channels. Squeezed (Sqz): cells passing through 7-μm microchannels. Statistical significance was determined by a one-way ANOVA and Tukey's multiple comparison test. The data represent the mean ± SD.

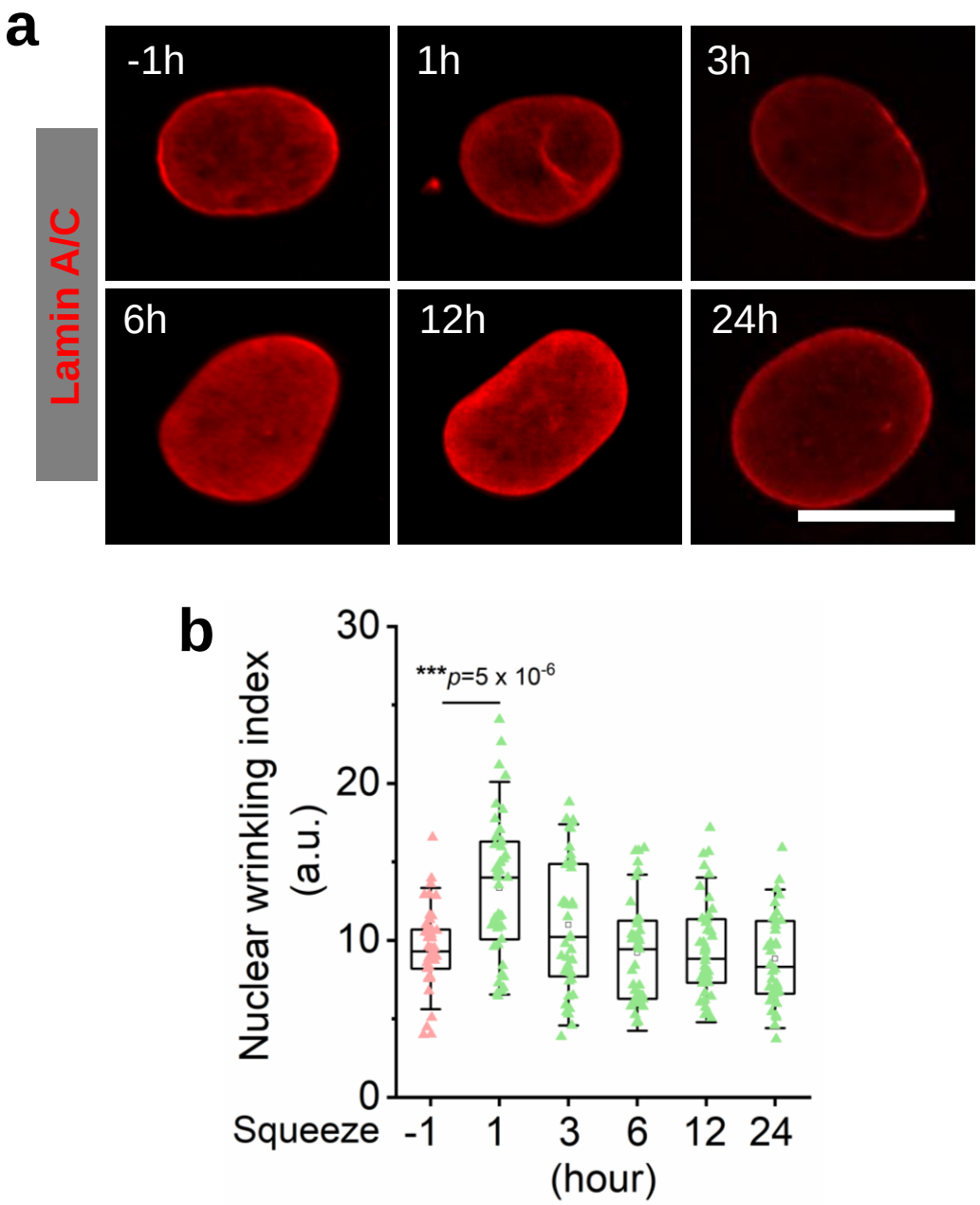

Supplementary Figure 34. Characterization of lamin A/C before and after mechanical deformation with 200-μm channels. (a) Representative images of lamin A/C staining in cells at the indicated time points before or after passing through 200-μm channels. Scale bar, 10 μm. **(b)** Quantification of nuclear wrinkling index at the indicated time points before and after mechanical squeezing with 200-μm channels (n=30 cells). Nuclear wrinkling was defined as the immunofluorescence intensity of wrinkles within the nuclear region. Statistical significance was determined by a one-way ANOVA and Tukey's multiple comparison test where all squeezed groups at indicated time points were compared with the before-squeezing group (-1 hour). In b, box plots show the ends at the quartiles, the mean as a horizontal line in the box, and the whiskers represent the SD.

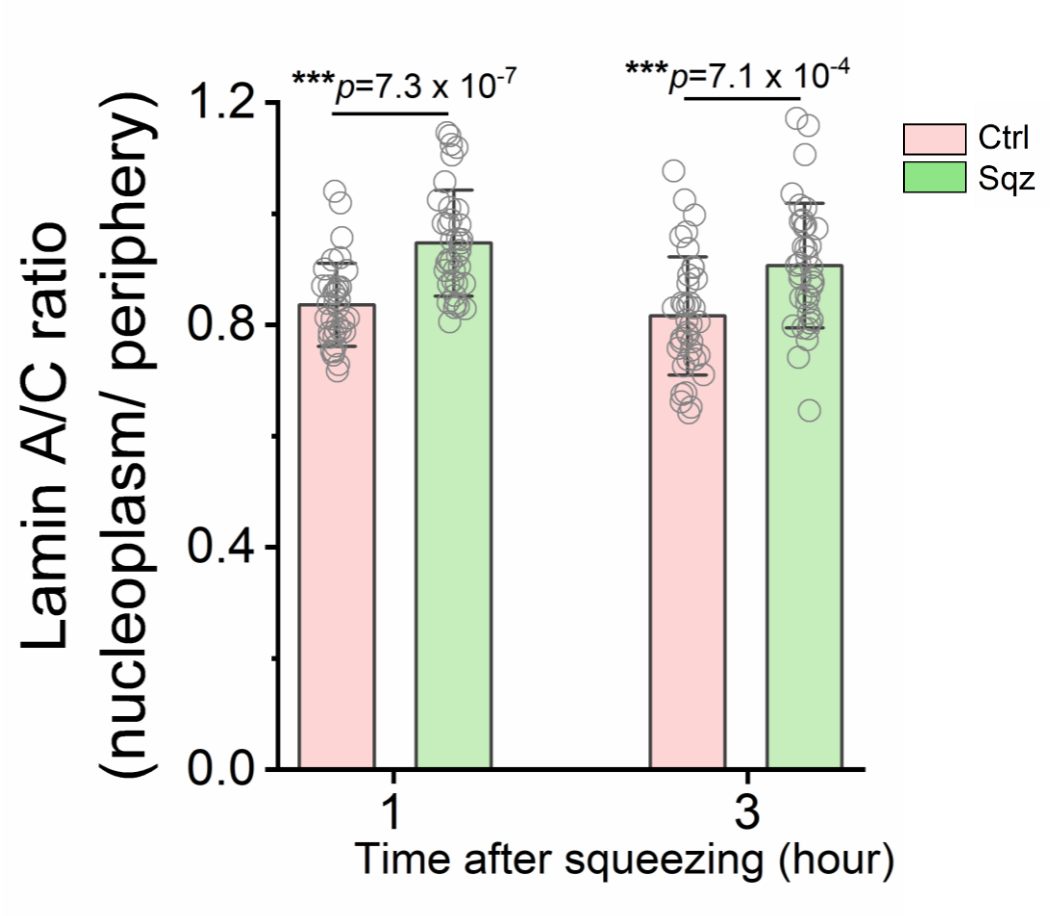

Supplementary Figure 35. Effect of microchannel-induced nuclear deformation on lamin A/C distribution. Quantification of nucleoplasm-to-periphery ratio of lamin A/C intensity in the nucleus based on immunofluorescent images of lamin A/C staining in control and squeezed cells at 1 hour and 3 hours after mechanical squeezing (n=35 cells). Control (Ctrl): cells passing through 200-μm channels. Squeezed (Sqz): cells passing through 7-μm microchannels. Statistical significance was determined by a two-tailed, unpaired t-test. The data represent the mean ± SD.

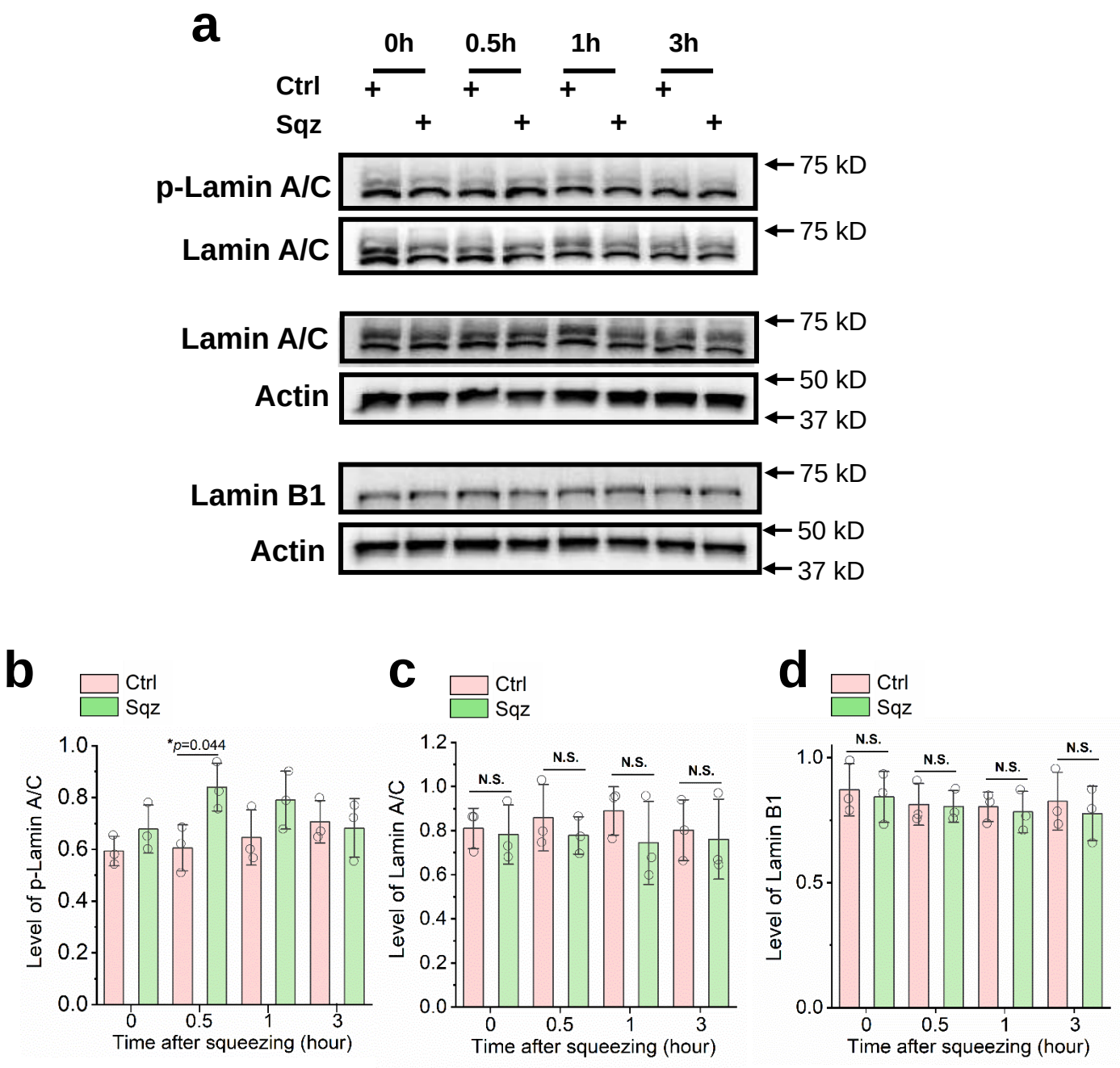

Supplementary Figure 36. Effect of microchannel deformation on lamin A/C phosphorylation. (a) Western blotting analysis of phospho-lamin A/C, lamin A/C, and lamin B1 levels in fibroblasts at the indicated time points after passing through the microchannels, where actin serves as a loading control. Quantification of phospho-lamin A/C levels (**b**), Lamin A/C levels (**c**) and lamin B1 levels (**d**) from Western blots (n=3). Statistical significance was determined by a two-tailed, unpaired t-test at each time point (NS: not significant), where the squeezed (Sqz) group was compared with the control (Ctrl) group. The data represent the mean ± SD.

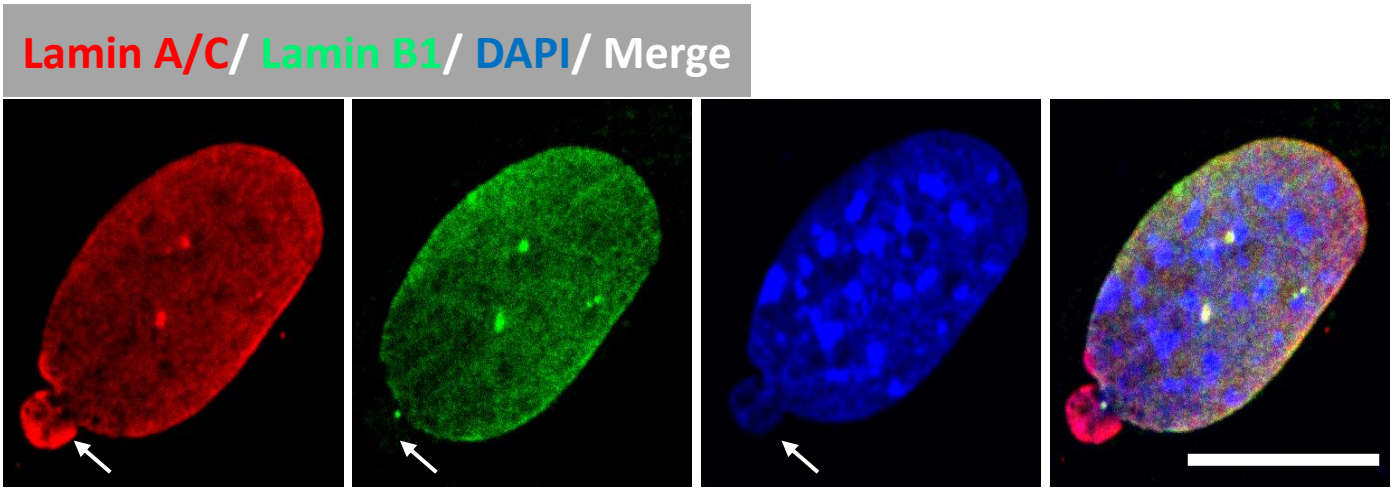

Supplementary Figure 37. Characterization of lamin A/C and lamin B1 after cells passed through 5-μm microchannels. Representative images of lamin A/C and lamin B1 staining in cells at 3 hours after passing through 5-μm microchannels. White arrows indicate the presence of lamin A/C but not lamin B1 in the blebbing region. Scale bar, 10 μm. Results were consistent across 3 independent experiments.

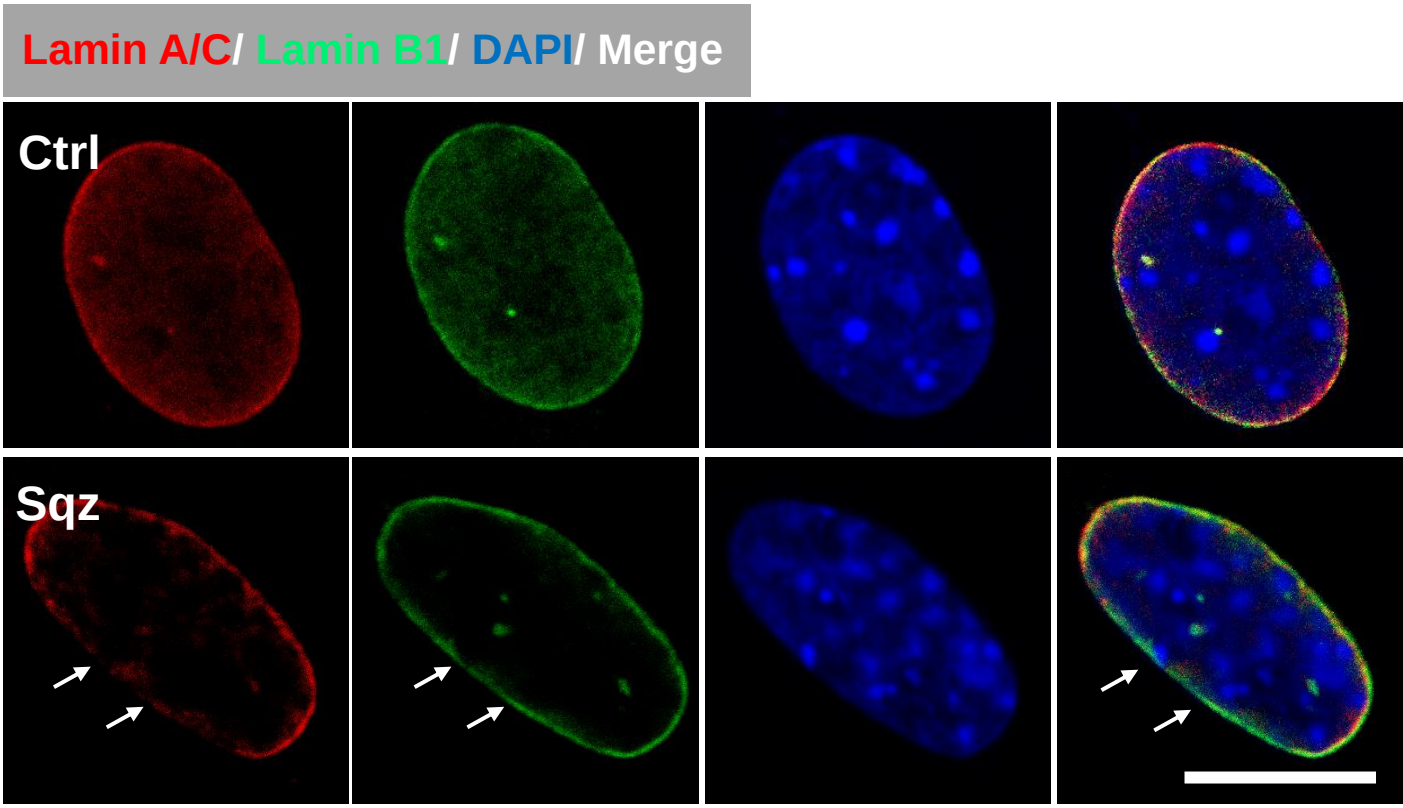

Supplementary Figure 38. Characterization of lamin A/C and lamin B1 after cells passed through 7-μm microchannels. Representative images of lamin A/C and lamin B1 staining in cells at 3 hours after passing through 7-μm microchannels. White arrows exemplify regions where there is a decrease in lamin A/C, but not lamin B1, at the nuclear periphery. Scale bar, 10 μm. Results were consistent across 3 independent experiments.

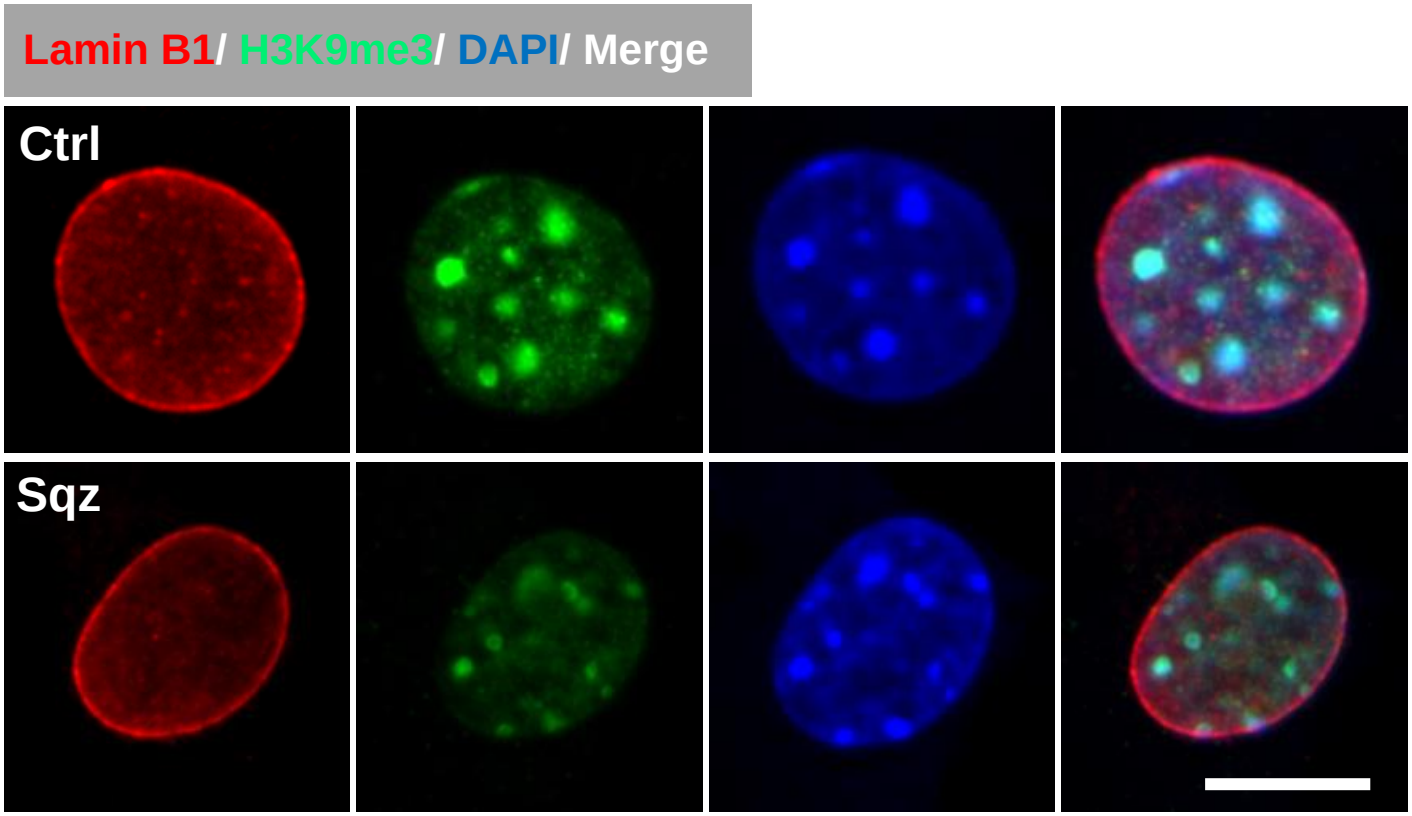

Supplementary Figure 39. Characterization of lamin B1 and H3K9me3 after cells passed through microchannels. Representative images of lamin B1 and H3K9me3 staining in cells at 3 hours after passing through 7-μm microchannels. Control (Ctrl): cells passing through 200-μm channels. Squeezed (Sqz): cells passing through 7-μm microchannels. Scale bar, 10 μm. Results were consistent across 3 independent experiments.

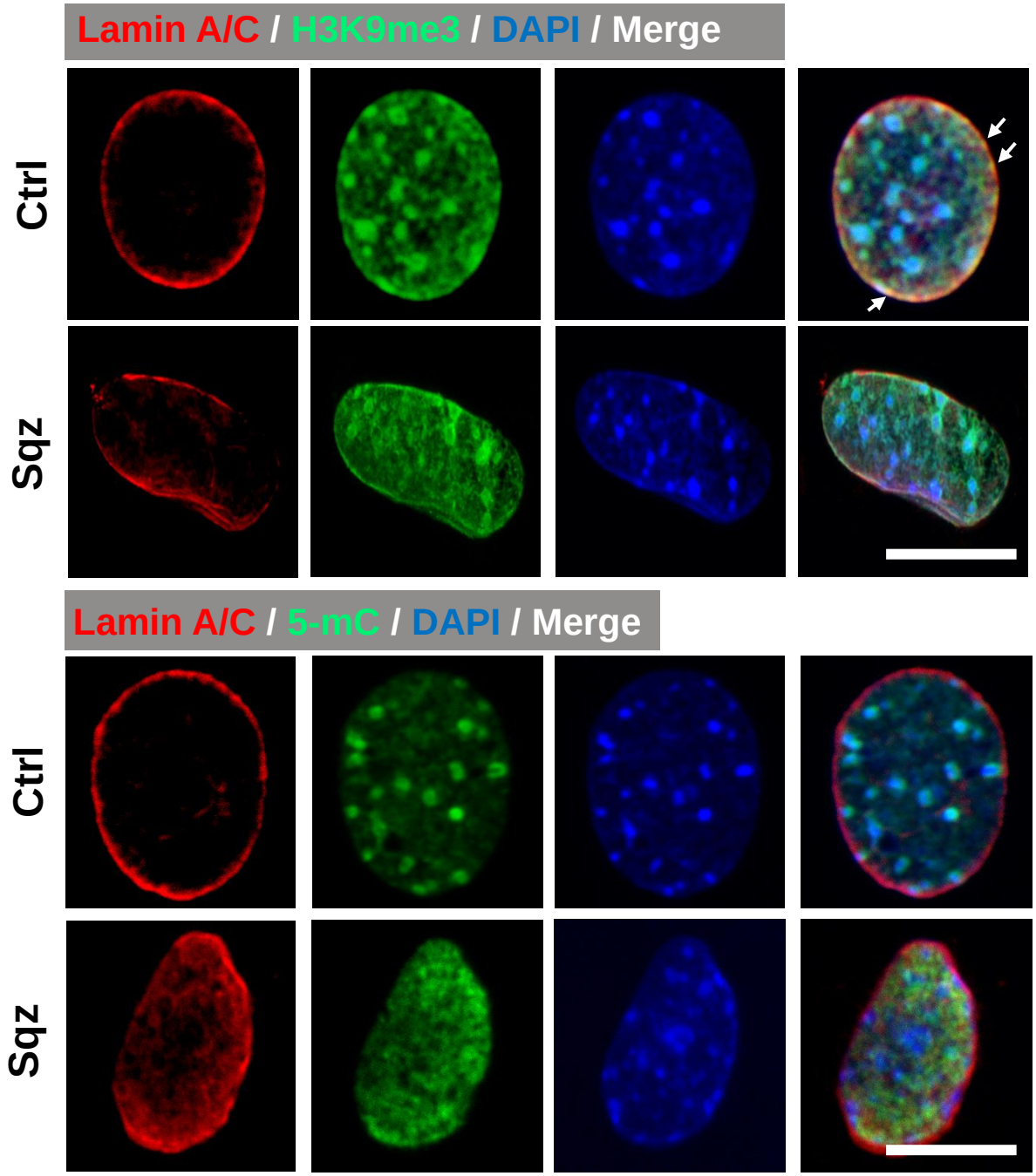

Supplementary Figure 40. Characterization of lamin A/C, H3K9me3 and 5-mC at 1 hour after cells passed through microchannels. Representative images of lamin A/C, H3K9me3, and 5-mC staining in cells at 1 hour after passing through 7-μm or 200-μm microchannels. Control (Ctrl): cells passing through 200-μm channels. Squeezed (Sqz): cells passing through 7-μm microchannels. White arrows exemplify the co-localization of lamin A/C and H3K9me3. Scale bar, 10 μm. Results were consistent across 3 independent experiments.

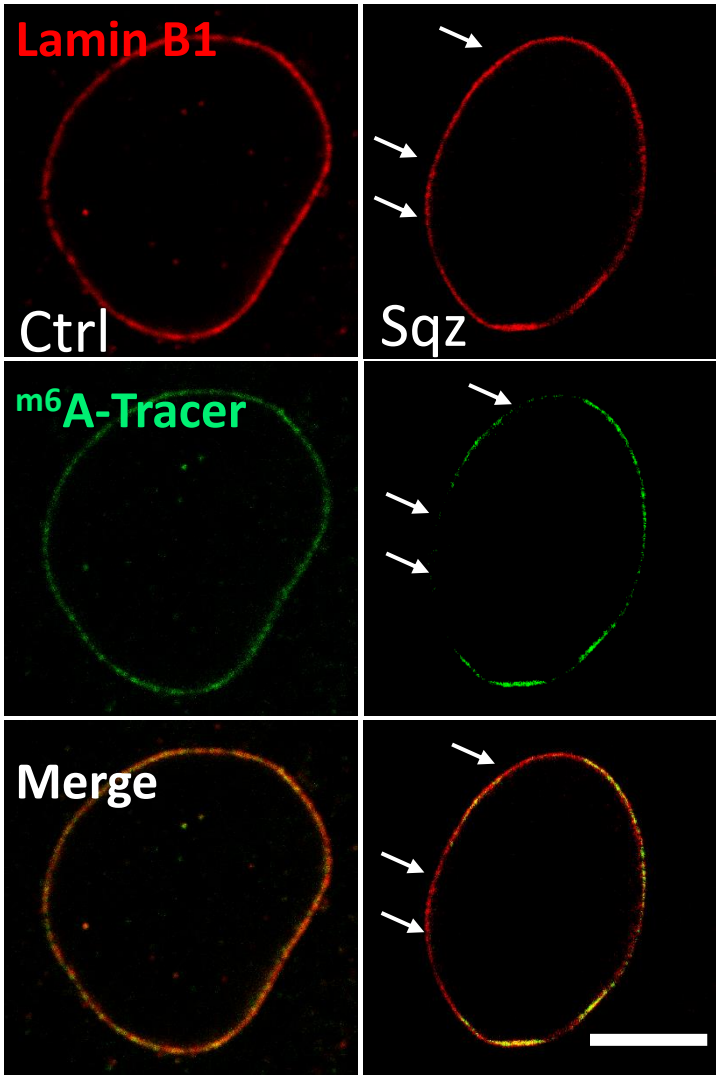

Supplementary Figure 41. Characterization of lamin B1 and ^{m6}A-tracer at 3 hours after cells passed through microchannels. Immunofluorescent images of lamin B1 and ^{m6A}-tracer in control and squeezed fibroblasts at 3 hours after mechanical deformation with the microchannels. Control (Ctrl): cells passing through 200-μm channels. Squeezed (Sqz): cells passing through 7-μm microchannels. White arrows exemplify regions where there is a decrease ^{m6}A-Tracer but not lamin B1, at the nuclear periphery. Scale bar, 5 μm. Results were consistent across 3 independent experiments.

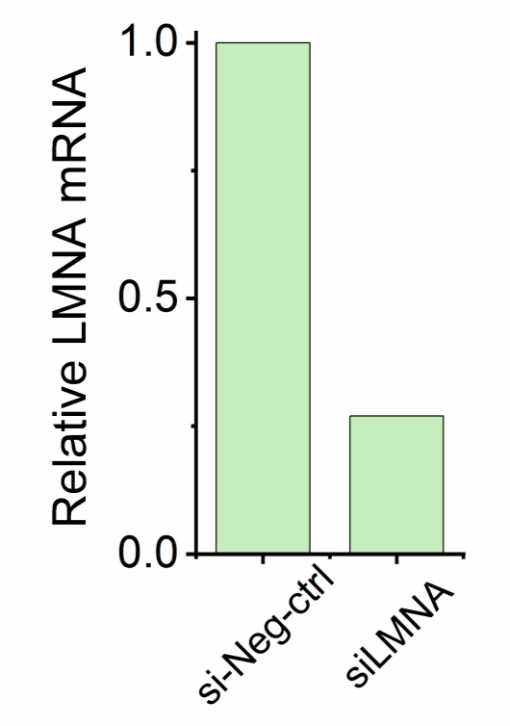

Supplementary Figure 42. Lamin A knockdown by using siRNA interference. Fibroblasts were transfected with an siRNA against lamin A (siLMNA) or a negative control siRNA (si-Neg-ctrl) respectively for 12 hours, and RNA was isolated from the samples after 1 day. The qRT-PCR analysis confirmed the successful knockdown of lamin A gene expression. Gene expression was normalized to 18S.

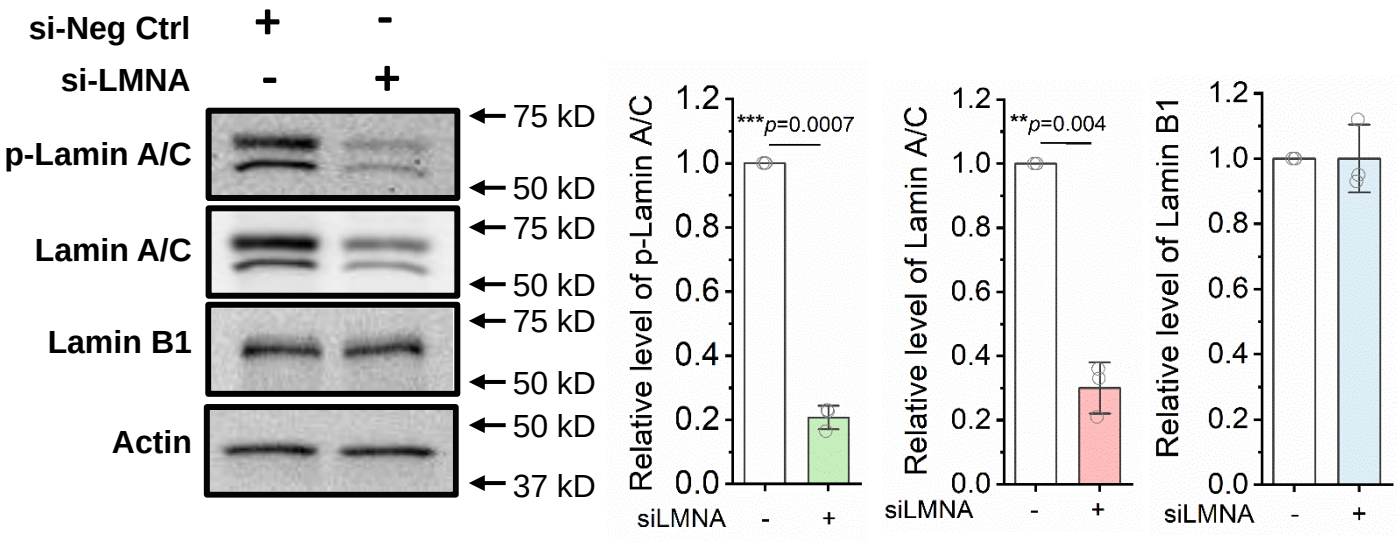

Supplementary Figure 43. Confirmation of lamin A/C knockdown by using siRNA interference. Fibroblasts were transfected with an siRNA against lamin A (*LMNA*) or negative control siRNA respectively for 12 hours. Total lysates were collected 48 hours after transfection, and Western blotting analysis was performed to detect phospho-lamin A/C, lamin A/C and lamin B1 protein. The results of phospho-lamin A/C, lamin A/C and lamin B1 from Western blots were quantified, where the lamin A silenced group was compared with the negative control group (n=3). statistical significance was determined by a two-tailed, unpaired t-test. The data represent the mean ± SD.

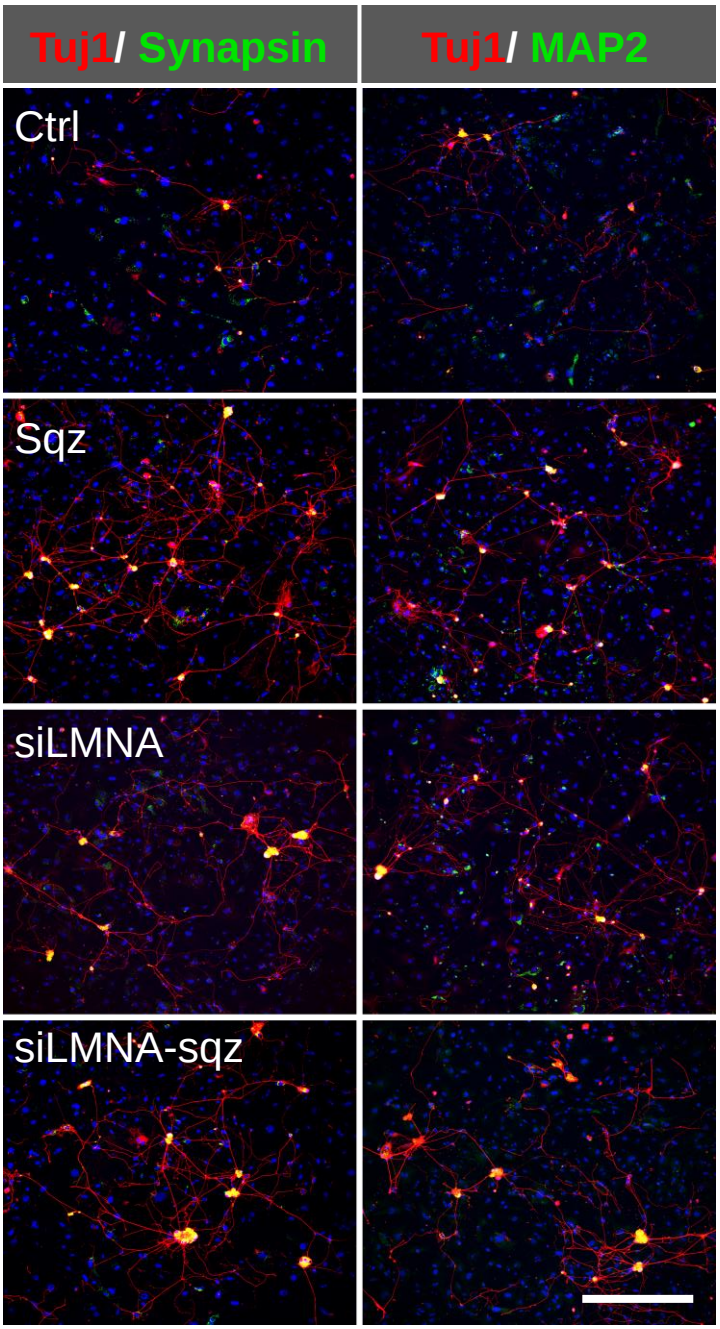

Supplementary Figure 44. Lamin A/C mediated iN reprogramming induced by mechanical squeezing. BAM-transduced fibroblasts were transfected with lamin A siRNA for 12 hours. Dox was added to culture media for 6 hours, and the cells were detached and introduced into 7-μm microchannels (Sqz). Cells passing through 200-μm channels were used as a control (Ctrl). Representative images of Tuj1 staining (Red), MAP2 (Green) and synapsin (Green) staining in control and lamin A-knockdown fibroblasts at 4 weeks after nuclear deformation. DNA was stained by DAPI (Blue). Scale bar, 200 μm. Results were consistent across 3 independent experiments.

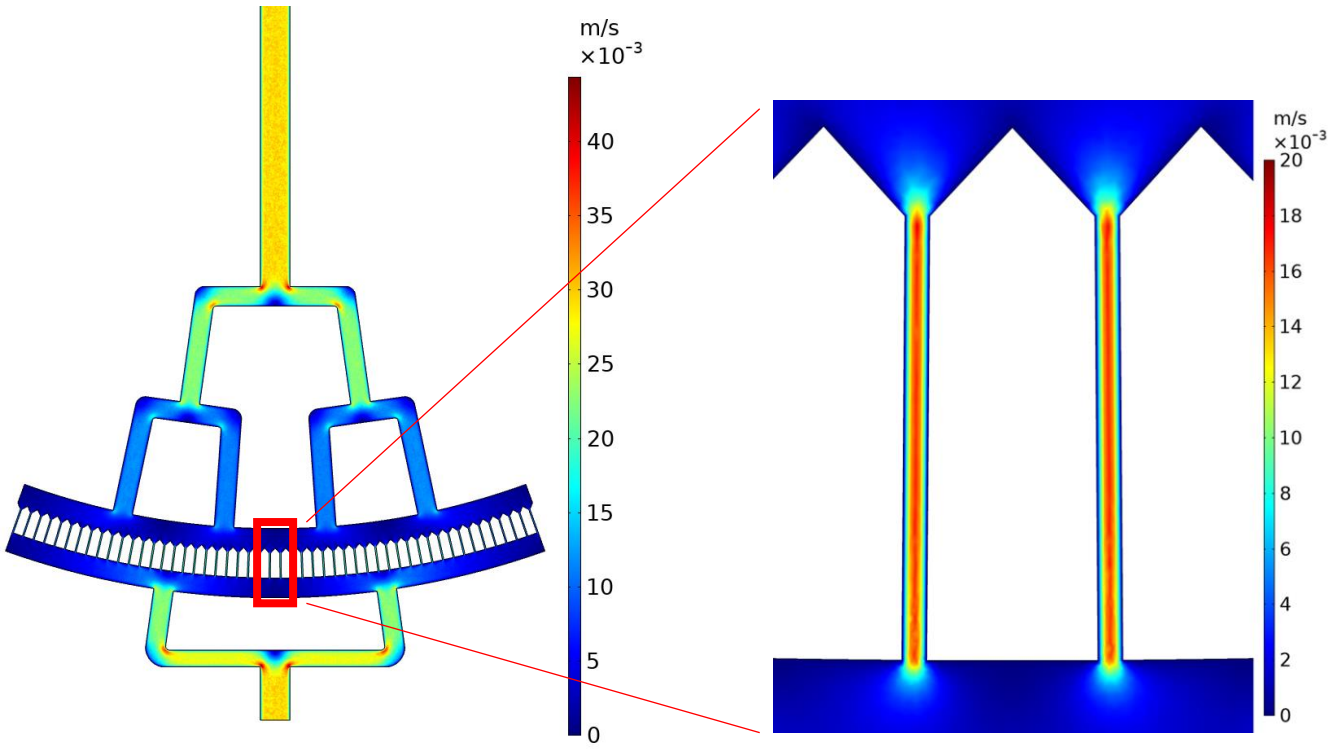

Supplementary Figure 45. Simulation of flow velocity magnitude in the high-throughput microfluidic device.

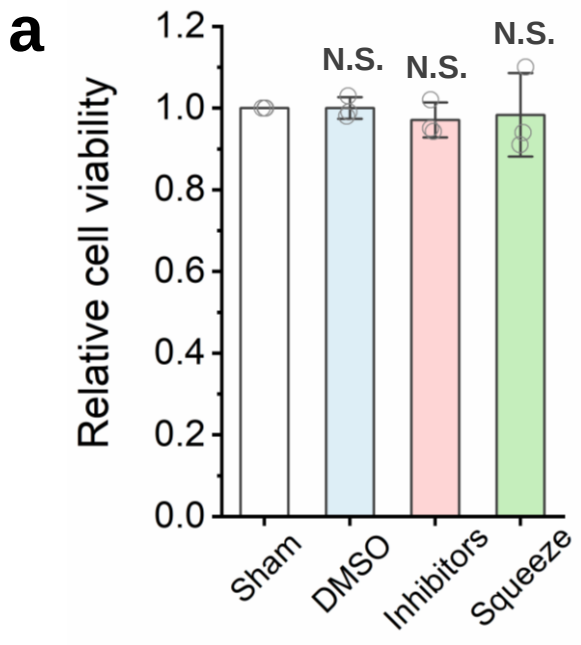

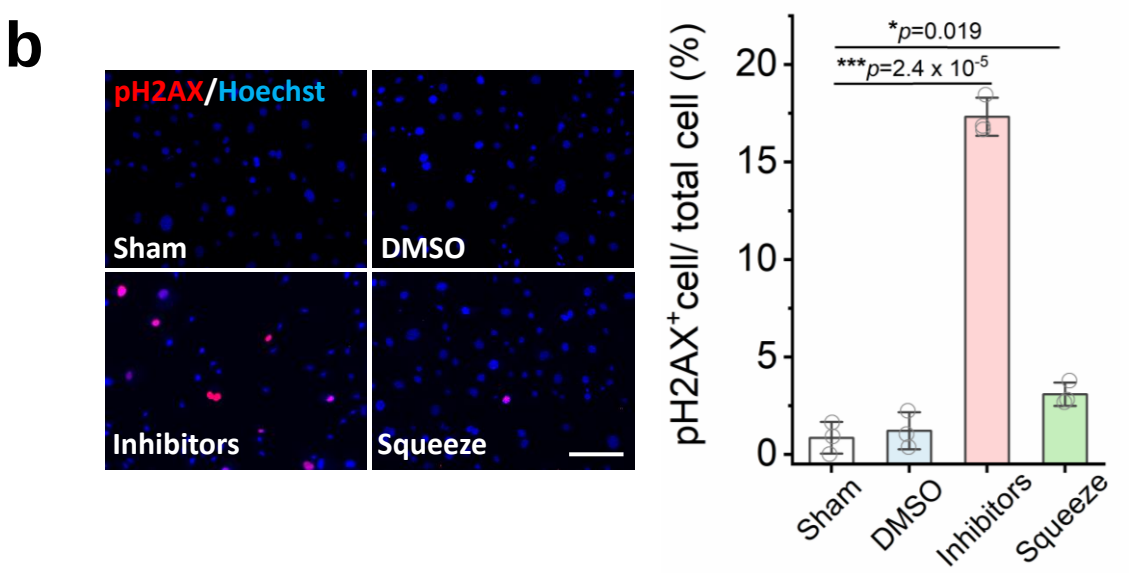

Supplementary Figure 46. Effect of microchannel-induced deformation and chemical inhibition on cell viability and DNA damage. (a) Quantification of cell viability in fibroblasts treated with Decitabine+Bix01294 (1:2) for 24 hours or in fibroblasts passing through 7-μm microchannels at 3 hours after re-plating onto glass slides, as determined using the PrestoBlue® Cell Viability Reagent. Cells were treated with DMSO as a solvent control, and sham refers to no treatment. All data were normalized to sham (n=3). Statistical significance was determined by a one-way ANOVA and Tukey's multiple comparison test (NS: not significant compared with control or sham, respectively). **(b)** Immunofluorescent staining for DNA damage in fibroblasts at 3 hours after passing through 7-μm microchannels or after a treatment with Decitabine+Bix01294 (1:2) for 24 hours as determined by the HCS DNA damage assay. Scale bar, 50 μm. The percentage of pH2Ax^{+} cells was based on immunofluorescent images (n=3). Statistical significance was determined by a one-way ANOVA and Tukey's multiple comparison test where all inhibitors-treated group, DMSO-treated group and squeezing group are compared with the sham group. The data represent the mean ± SD.

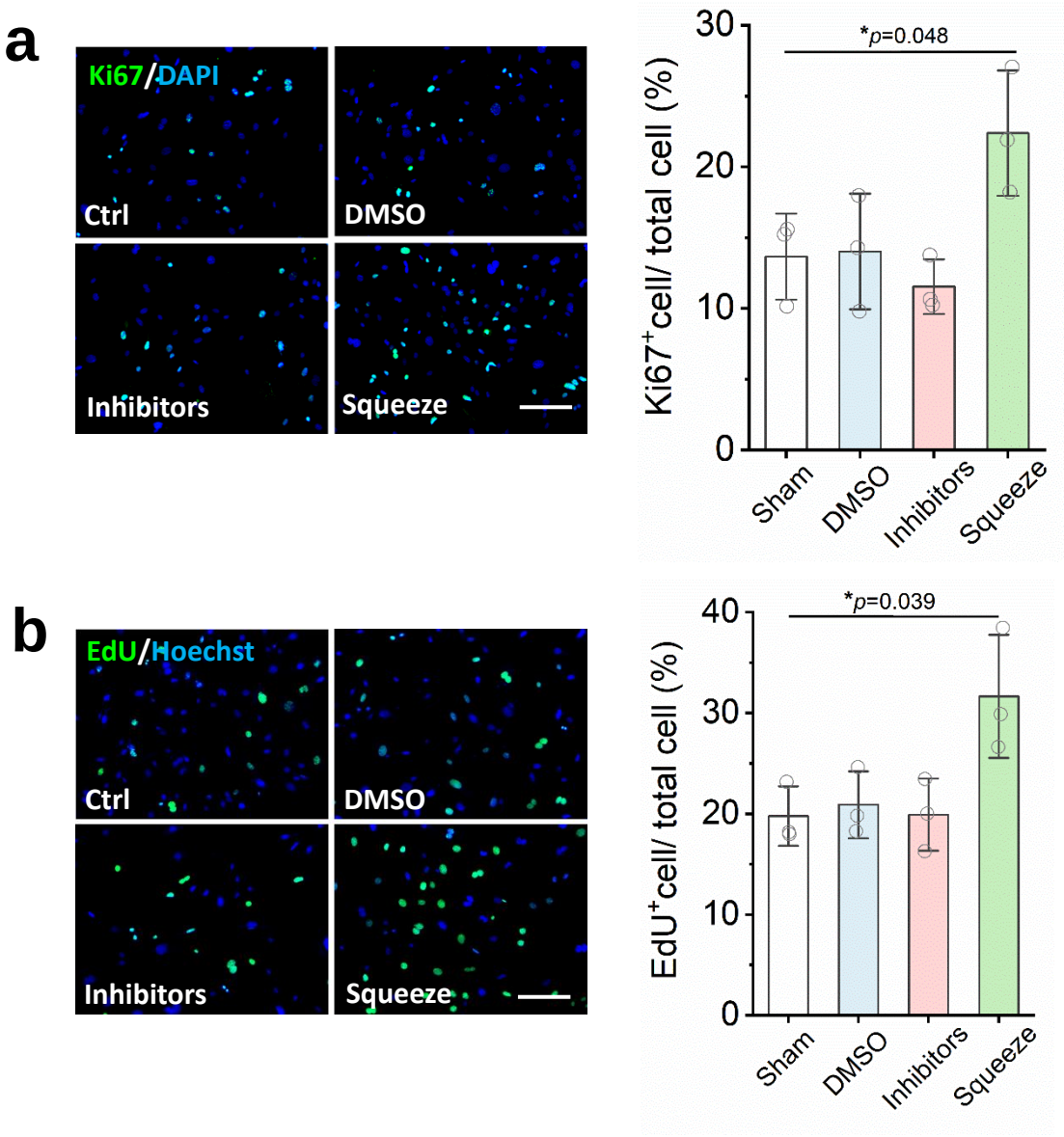

Supplementary Figure 47. Effect of microchannel-induced deformation and chemical inhibition on cell proliferation. Immunofluorescent images show Ki67 staining (**a**) or EdU labeling (**b**) in fibroblasts treated with Decitabine+Bix01294 (1:2) for 24 hours or in fibroblasts passing through 7-μm microchannels followed by 24-hour culture. Scale bar, 50 μm. Quantification of the percentage of $Ki67^+$ (**a**) or EdU^+ (**b**) cells based on immunofluorescent images (n=3). Statistical significance was determined by a one-way ANOVA and Tukey's multiple comparison test, where all groups were compared with the sham group. The data represent the mean ± SD.

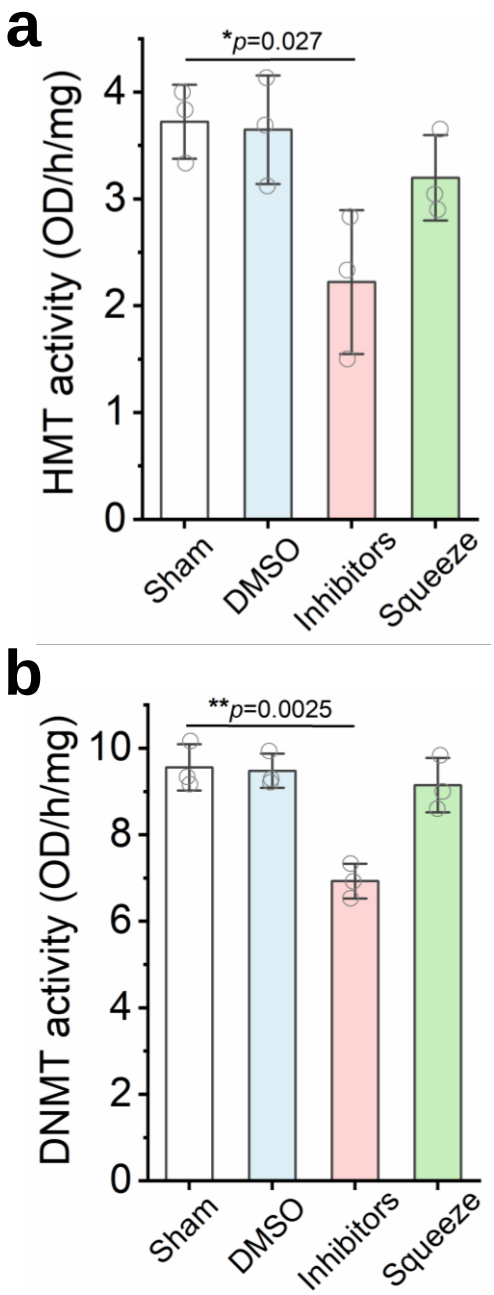

Supplementary Figure 48. Effect of microchannel-induced deformation and chemical inhibition on HMT and DNMT activity. Quantification of HMT **(a)** and DNMT **(b)** activity in fibroblasts treated with Decitabine+Bix01294 (1:2) for 24 hours or in fibroblasts passing through 7-μm microchannels followed by 3-hour culture, as determined by EpiQuik Histone Methyltransferase Activity/Inhibition Assay Kit (H3K9) and EpiQuik DNMT Activity/Inhibition Assay Ultra Kit (EpiQuik, USA) (n=3). Cells were treated with DMSO as solvent control, and sham refers to no treatment. Statistical significance was determined by a one-way ANOVA and Tukey's multiple comparison test, where all groups were compared with the sham group. The data represent the mean ± SD.

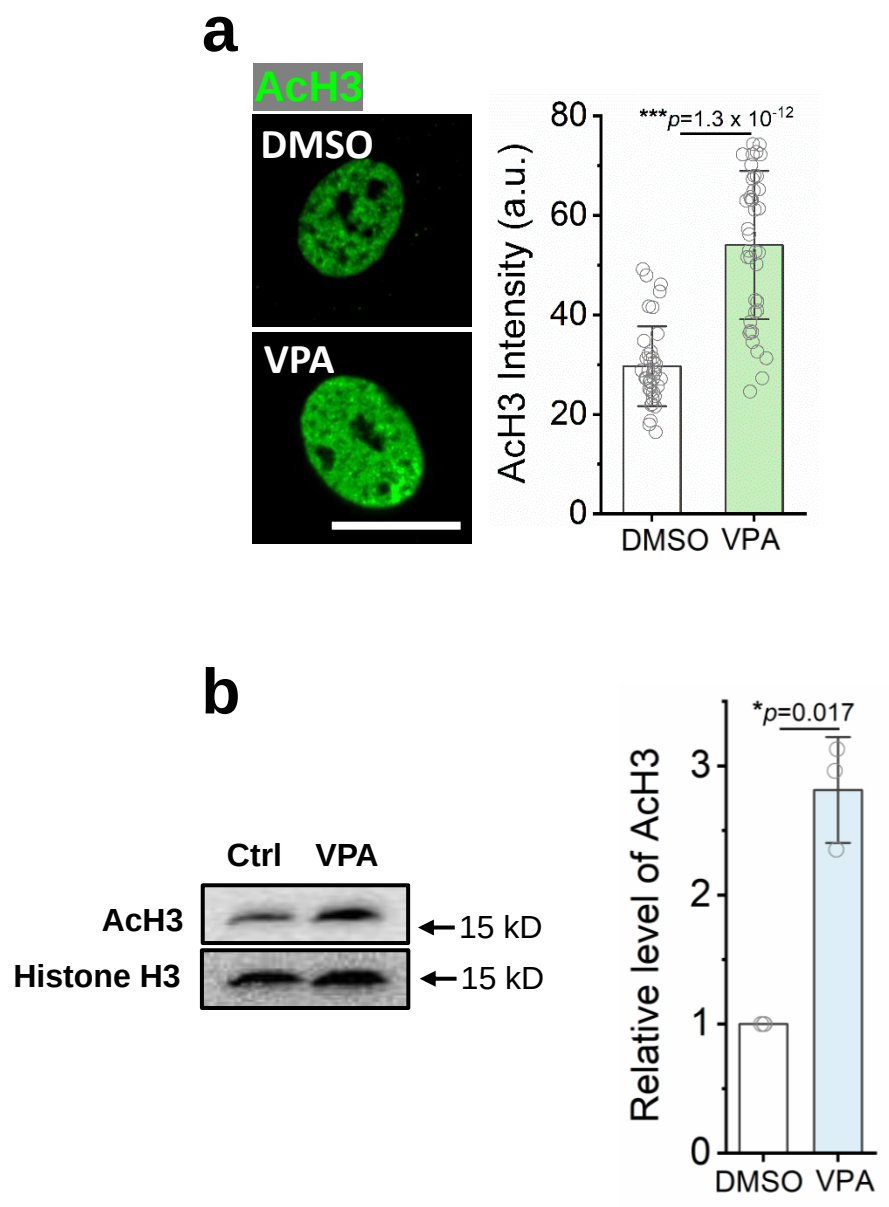

Supplementary Figure 49. Characterization of histone deacetylase (HDAC) inhibition. (a) Immunofluorescent images show AcH3 in fibroblasts treated with or without 0.5 mM HDAC inhibitor Valproic acid (VPA) for 24 hours. Fibroblasts treated with DMSO served as a solvent control. Scale bar, 10 μm. AcH3 intensity was quantified based on immunofluorescent images, a.u.: arbitrary unit (n=40 cells). Statistical significance was determined by a two-tailed, unpaired t-test. **(b)** Western blotting was used to examine the levels of AcH3 in fibroblasts treated with VPA or DMSO for 24 hours, where histone H3 served as a loading control. Relative levels of AcH3 were quantified based on Western blots (n=3). Statistical significance was determined by a two-tailed, unpaired t-test, where VPA-treated groups were compared with the control (DMSO) group. The data represent the mean ± SD.

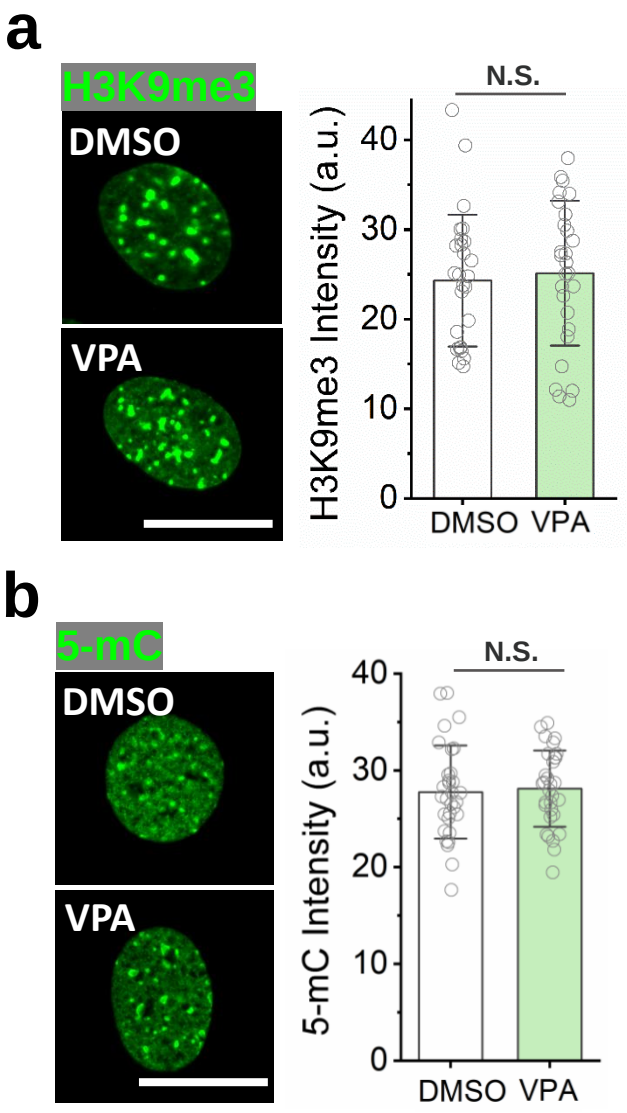

Supplementary Figure 50. Effect of HDAC inhibition on H3K9me3 and 5-mC. Fibroblasts were treated with DMSO (solvent control) or HDAC inhibitor VPA for 24 hours. Cells were fixed and stained for H3K9me3 (**a**) or 5-mC (**b**). Representative immunofluorescent images were collected by fluorescence microscopy. Scale bar, 10 µm. The levels of H3K9me3 (a) and 5-mc (b) were quantified based on immunofluorescent images, a.u.: arbitrary unit (n=30 cells). Statistical significance was determined by a two-tailed, unpaired t-test (NS: not significant, where VPA-treated groups were compared with the control (DMSO) group. The data represent the mean ± SD.

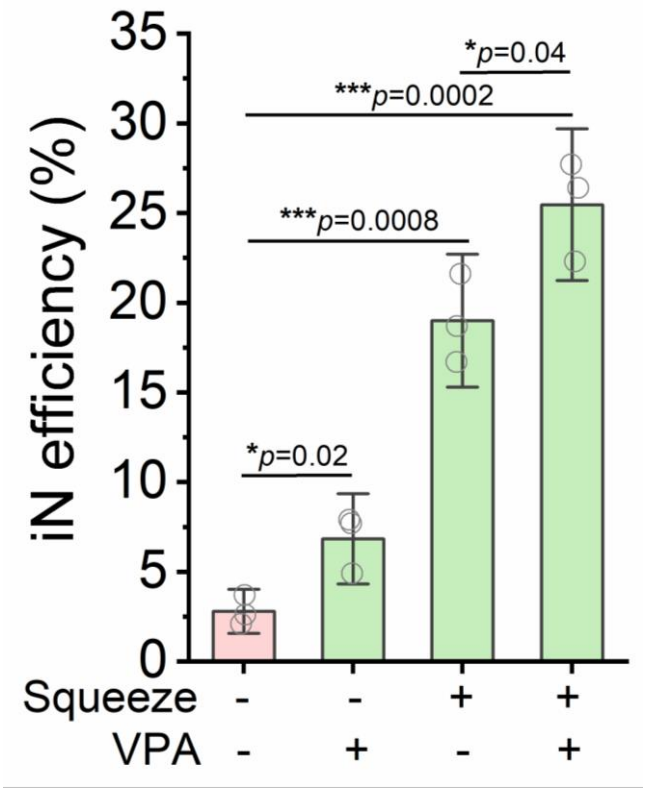

Supplementary Figure 51. Effect of HDAC inhibition on iN reprogramming efficiency. BAM-transduced fibroblasts were pretreated with HDAC inhibitor VPA (0.5 mM) for 24 hours before passing through 7-μm microchannels. After cells passed through the microdevice, BAM-transduced fibroblasts were seeded on fibronectin-coated glass slides and cultured in N2B27 medium for 7 days. At day 7, the cells were fixed and stained for Tubb3 by using a Tuj1 antibody, followed by immunofluorescence microscopy to quantify $Tuj1^{+}$ iN cells. The reprogramming efficiency was determined based on Tuj1 staining (n=3). Cells passing through 200-μm channels were used as a control. Statistical significance was determined a one-way ANOVA and Tukey's multiple comparison test, where VPA-treated and squeezed groups were compared with the control group. The data represent the mean ± SD.

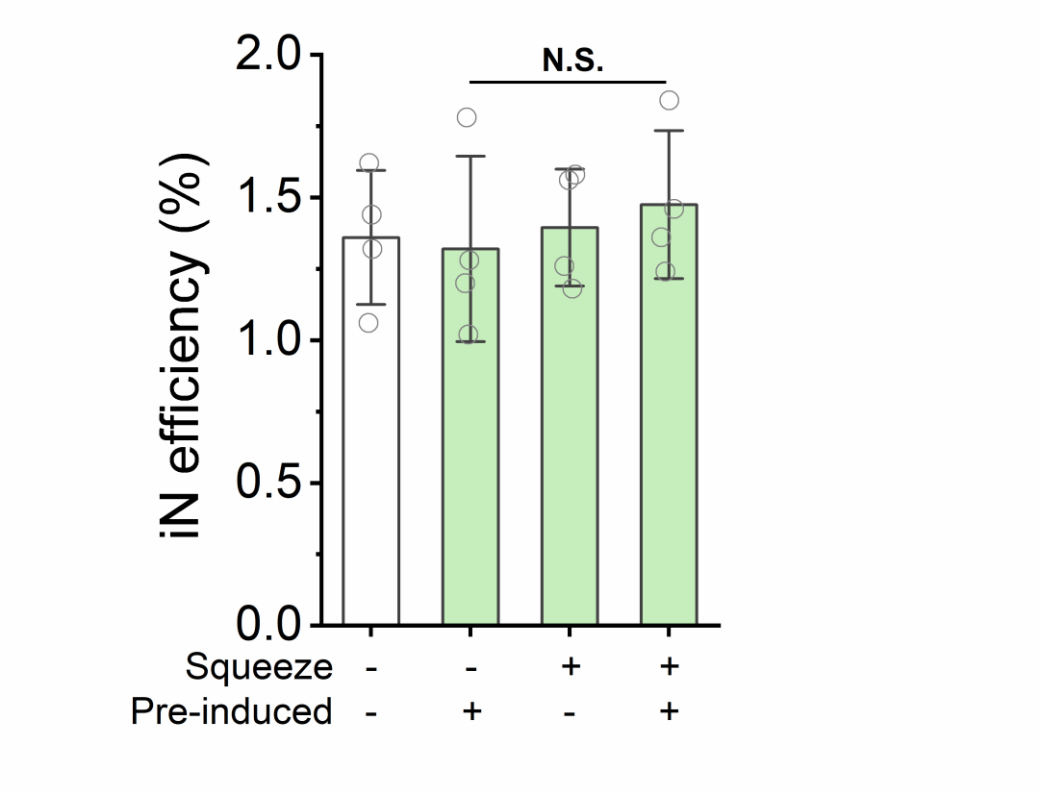

Supplementary Figure 52. Microfluidic deformation has no significant effect on chemical induced-iN reprogramming. Fibroblasts were treated with small molecule cocktail (Forskolin, CHIR99012, ISX9 and IBET-151) or solvent control for one day before mechanical squeezing (pre-induced), and cultured for 21 days after mechanical squeezing in the presence of the chemical cocktail, at which point the reprogramming efficiency of chemically induced neurons was determined (n=4). Statistical significance was determined a one-way ANOVA and Tukey's multiple comparison test (NS: not significant). The data represent the mean ± SD.

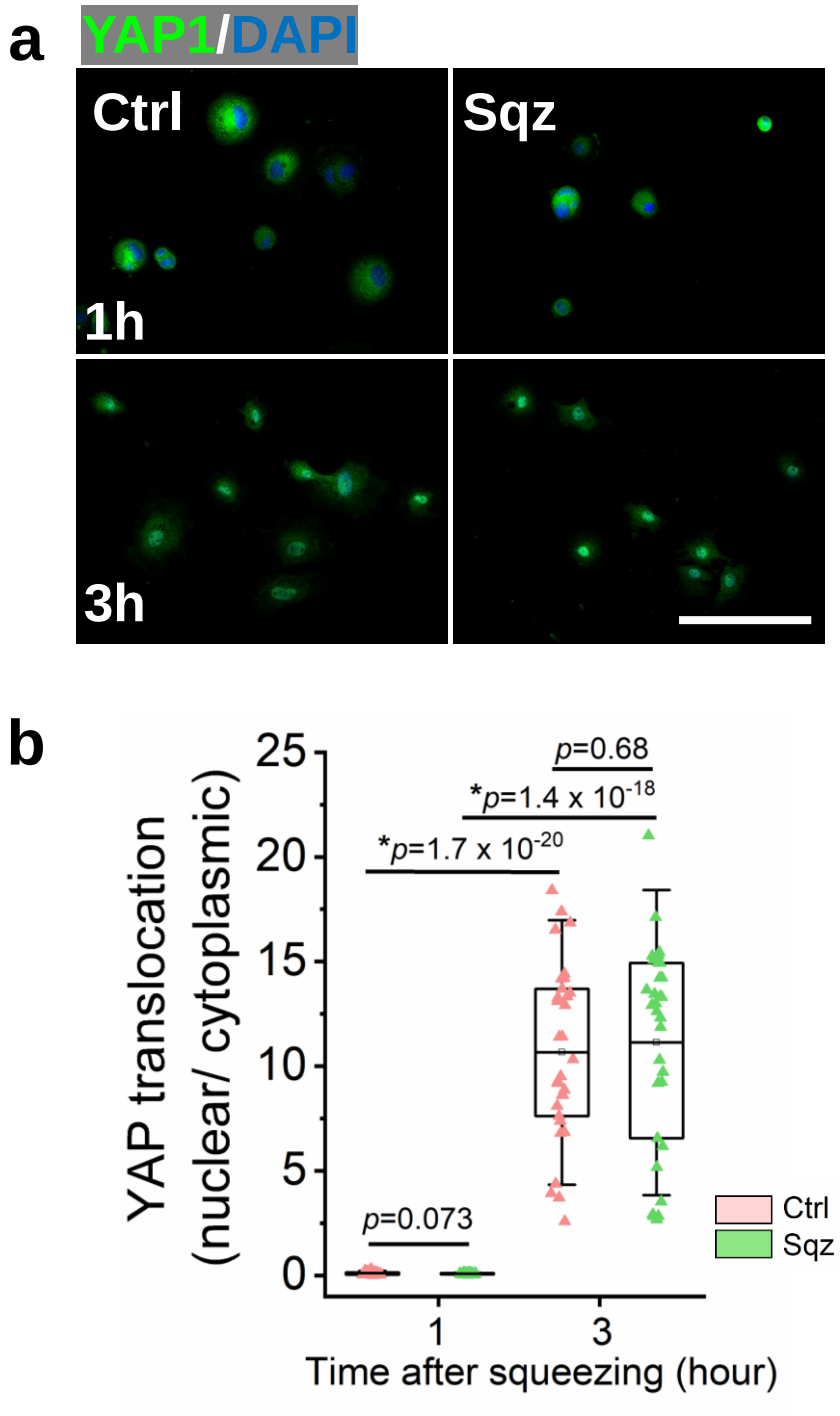

Supplementary Figure 53. Effect of mechanical squeezing on YAP localization. Representative immunofluorescent images of YAP in fibroblasts at the indicated time points after cells passed through the microchannels. Control (Ctrl): cells passing through 200-μm channels. Squeezed (Sqz): cells passing through 7-μm microchannels. Scale bar, 100 μm. **(b)** Quantification of the nuclear-to-cytoplasmic ratio of YAP based on immunofluorescent images in (**a**) (n= 30 cells). Statistical significance was determined a one-way ANOVA and Tukey's multiple comparison test, where the squeezed group (Sqz) was compared with the control group (Ctrl). In b, box plots show the ends at the quartiles, the mean as a horizontal line in the box, and the whiskers represent the SD.

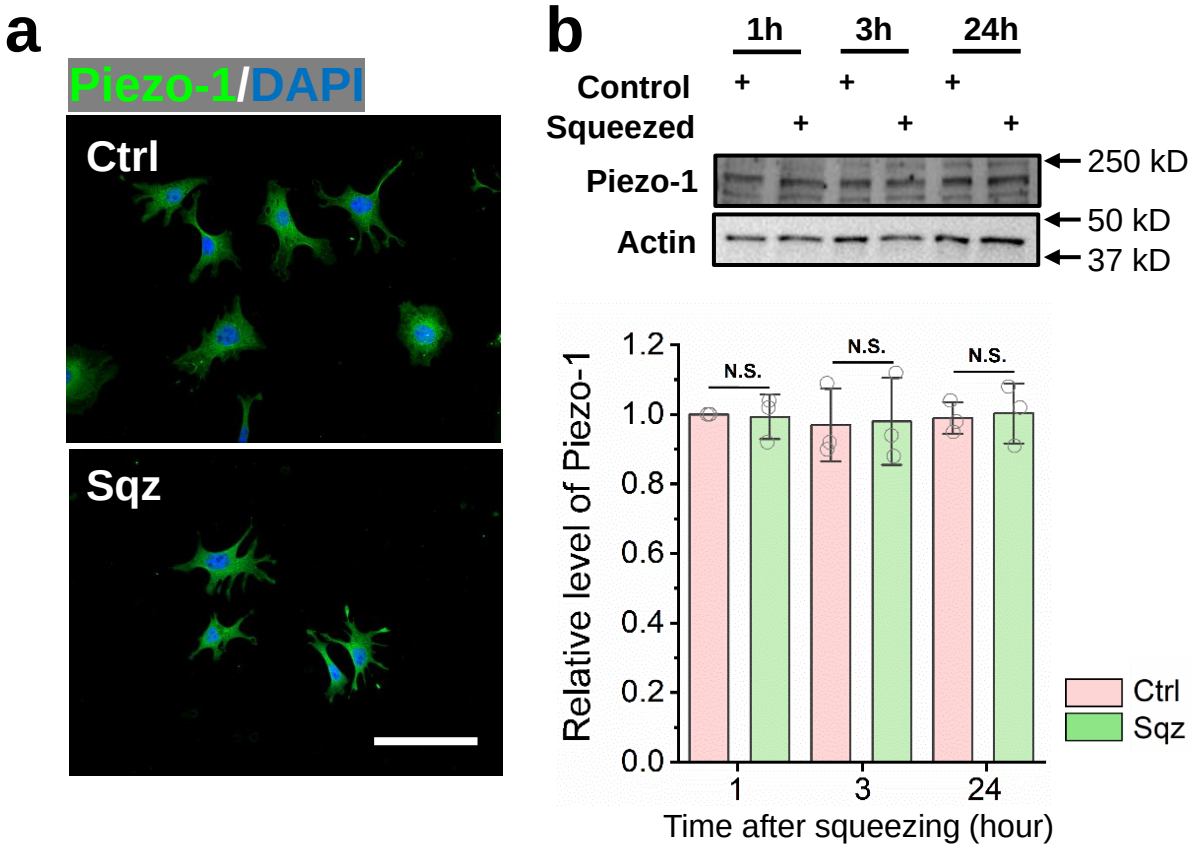

Supplementary Figure 54. Effect of microfluidic deformation on Piezo-1 level. (a) Representative immunofluorescent images of Piezo-1 staining in cells at 3 hours after passing through the microchannels. Control (Ctrl): cells passing through 200-μm channels. Squeezed (Sqz): cells passing through 7-μm microchannels. Scale bar, 50 μm. **(b)** Western blot analysis of Piezo-1 expression in control and squeezed cells at the indicated time points after microchannel-induced deformation, where actin serves as a loading control. Piezo-1 levels were quantified from Western blots (n=3). Statistical significance was determined by a two-tailed, unpaired t-test at each time point (NS: not significant), where the squeezed group (Sqz) was compared with the control group (Ctrl). The data represent the mean ± SD.

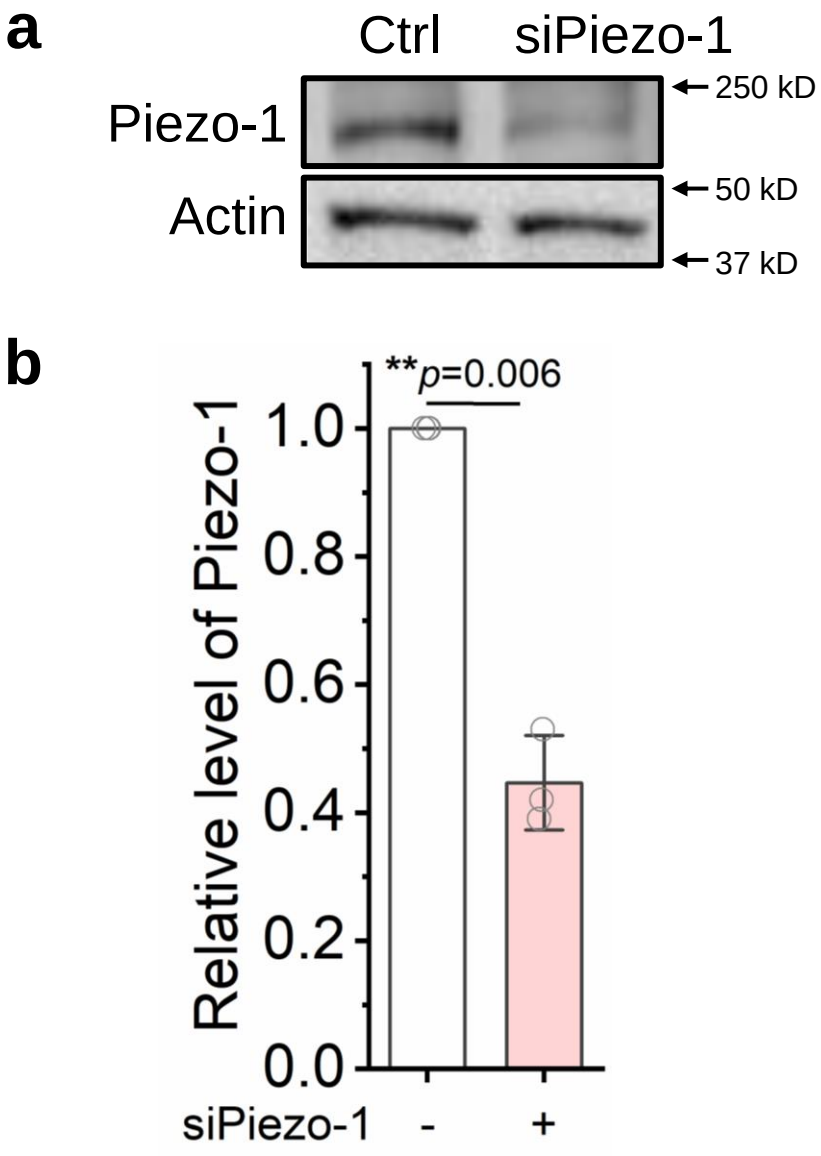

Supplementary Figure 55. Piezo-1 knockdown using siRNA interference. (a) Western blotting was used to examine the levels of Piezo-1 in control and Piezo-1 silenced fibroblasts at 48 hours after knockdown. **(b)** Quantification of Piezo-1 levels from Western blots (n=3). Statistical significance was determined by a two-tailed, unpaired t-test. The data represent the mean ± SD.

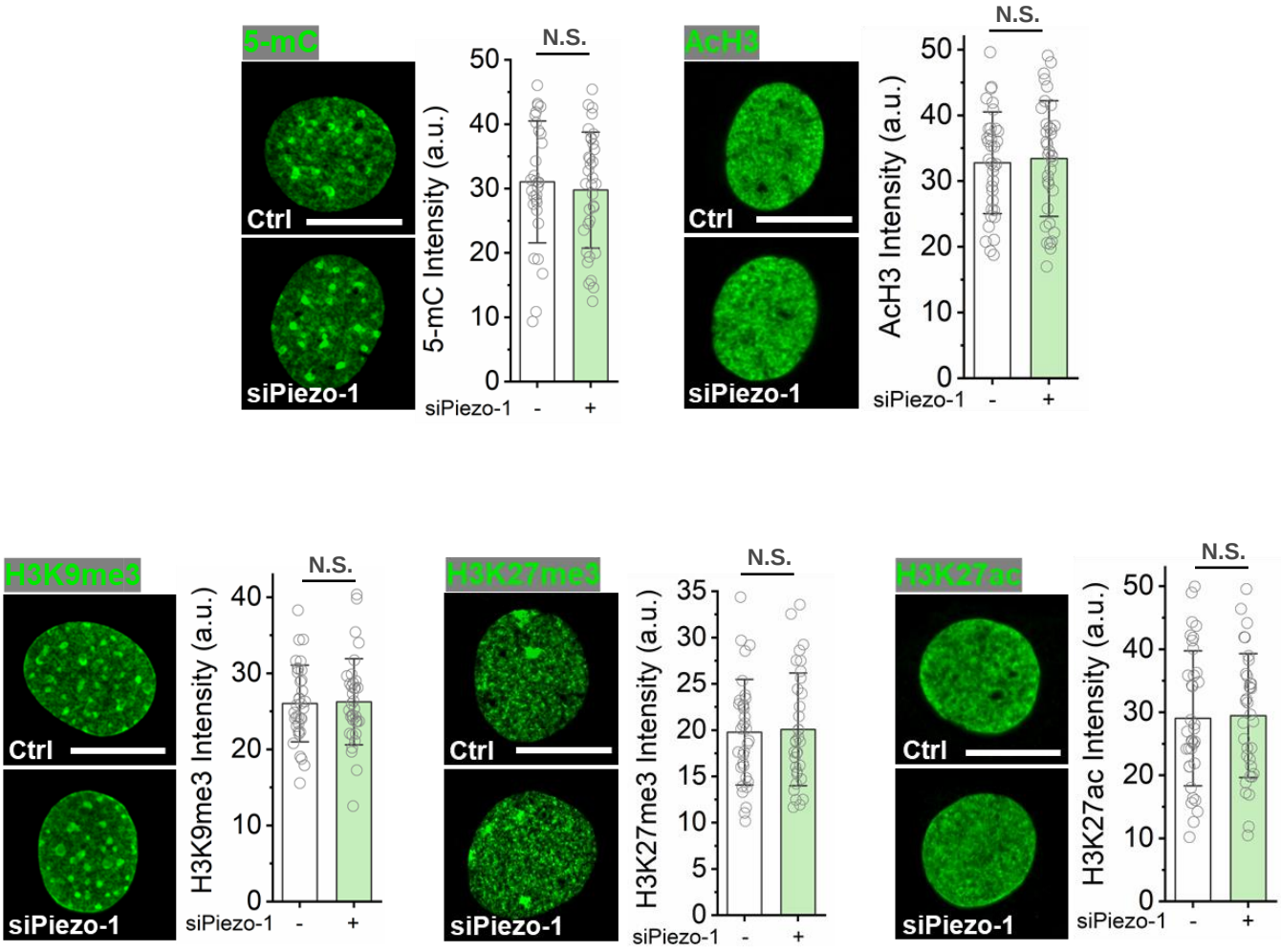

Supplementary Figure 56. Effect of Piezo-1 knockdown on DNA methylation and histone marks. Fibroblasts were transfected with an siRNA against Piezo-1 for 12 hours, and samples were fixed and stained 48 hours after transfection. Representative immunofluorescent images show the level and distribution of various histone marks in control and Piezo-1-silenced BAM-transduced fibroblasts. Scale bar, 10 µm. The histone mark intensity was quantified based on immunofluorescent images (n=30 cells). Statistical significance was determined by a two-tailed, unpaired t-test (NS: not significant), where the Piezo-1 silenced group was compared with the negative control group. The data represent the mean ± SD.

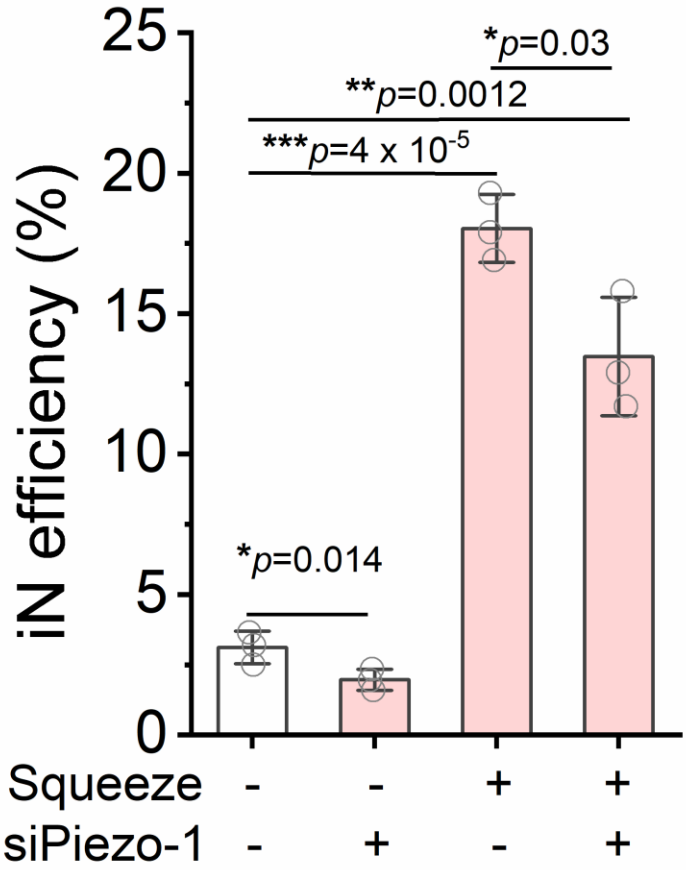

Supplementary Figure 57. Effect of Piezo-1 knockdown on microchannel-induced iN reprograming. BAM-transfected fibroblasts were transfected with siRNA against Piezo-1 for 12 hours, and 48 hours after transfection, cells were introduced into 7-μm microchannels. After cells passed through the microdevice, fibroblasts were seeded on fibronectin-coated glass slides and cultured in N2B27 medium for 7 days. At day 7, the cells were fixed and stained for Tubb3 by using Tuj1 antibody, followed by immunofluorescence microscopy to quantify $Tuj1^{+}$ iN cells. The reprogramming efficiency was determined based on Tuj1 staining (n=3). Cells passing through 200-μm channels were used as a control. Statistical significance was determined by a one-way ANOVA and Tukey's multiple comparison test, where siPiezo-1 and squeezed groups were compared with no-treatment group (white bar). The data represent the mean ± SD.

Supplementary Table 1. Antibodies used for immunocytochemistry and Western blotting analysis

Antibody	Vendor	Catalog #	Dilution
Tuj1	Biolegend	801202	1:1000 (IF)
H3K4me1	Abcam	ab32356	1:300 (IF)
H3K9me3	Abcam	ab8898	1:500 (IF)/ 1:1000 (WB)
H4K20me3	Abcam	ab4729	1:300 (IF)
H3K27me3	Abcam	ab192985	1:300 (IF))/ 1:1000 (WB)
AcH3	Millipore	06-599	1:300 (IF)/ 1:1000 (WB)
H3K9ac	Abcam	ab4441	1:300 (IF)
5-mC	Cell signaling	28692S	1:500 (IF)
Synapsin	Abcam	ab64581	1:100 (IF)
MAP-2	Sigma	M9942	1:200 (IF)
Lamin A/C	Santa Cruz	sc-376248	1:50 (IF)
Histone H3	Abcam	ab1791	1:2000 (WB)
Lamin B1	Santa Cruz	sc-374015	1:50 (IF)
Lamin B1	Abcam	ab133741	1:1000 (WB)
YAP1	Santa Cruz	sc-376830	1:100 (IF)
Piezo-1	ThermoFisher	15939-1-AP	1:200 (IF)/ 1:1000 (WB)
Phospho-Lamin A/C	ThermoFisher	PA5-17113	1:200 (IF)/ 1:1000 (WB)
Ki67	Abcam	ab16667	1:200 (IF)
Nanog	Abcam	ab214549	1:300 (IF)

Supplementary Fig 16

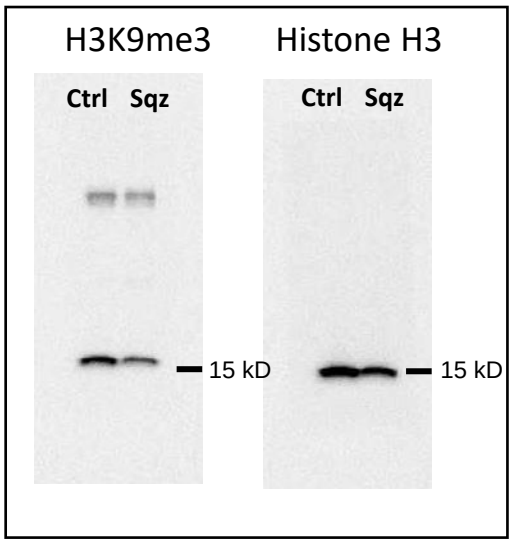

Supplementary Fig 21

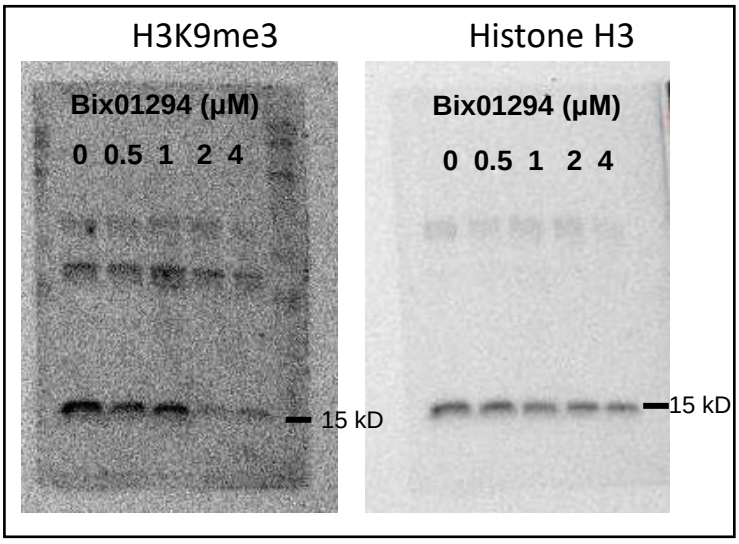

Supplementary Fig 18

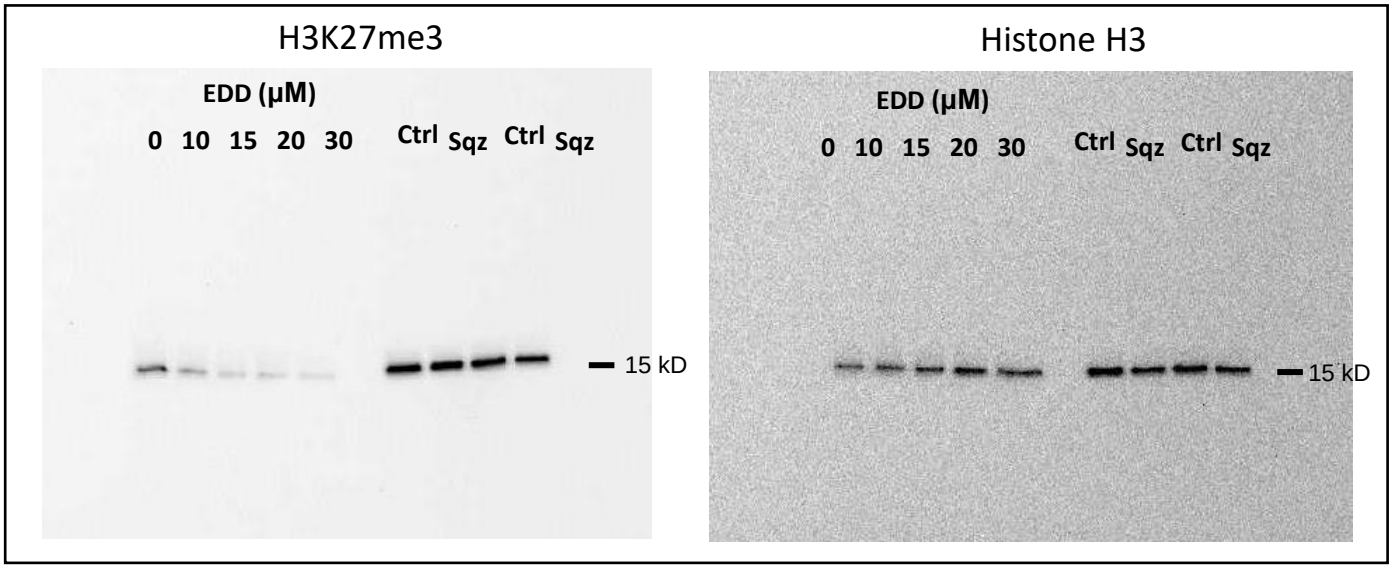

Supplementary Fig 49

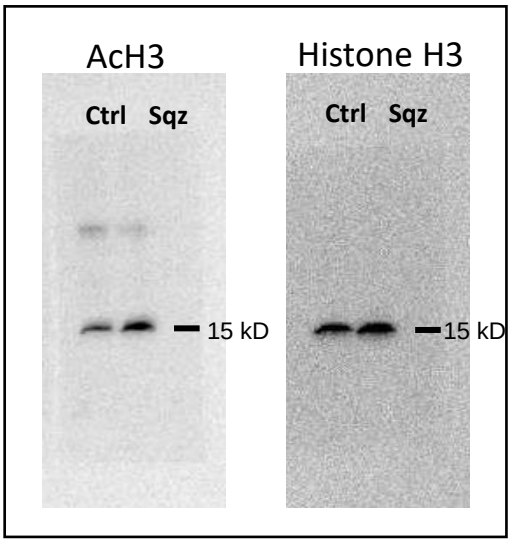

Supplementary Fig 36

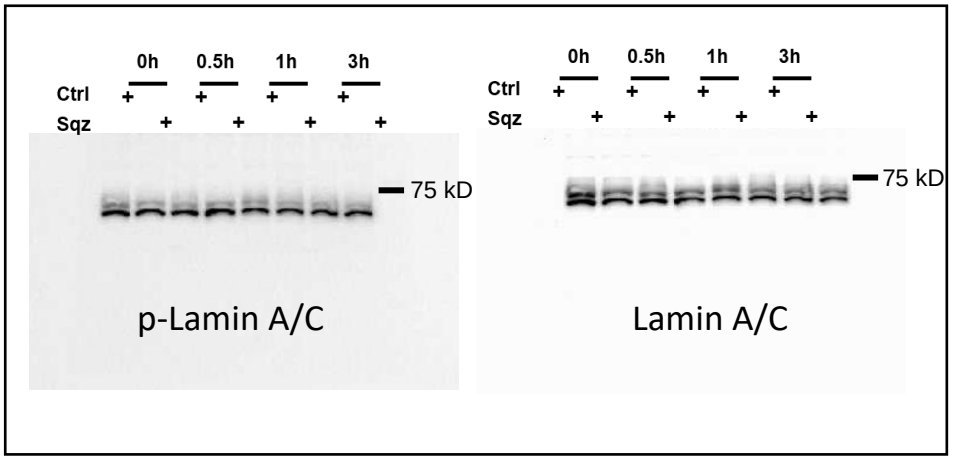

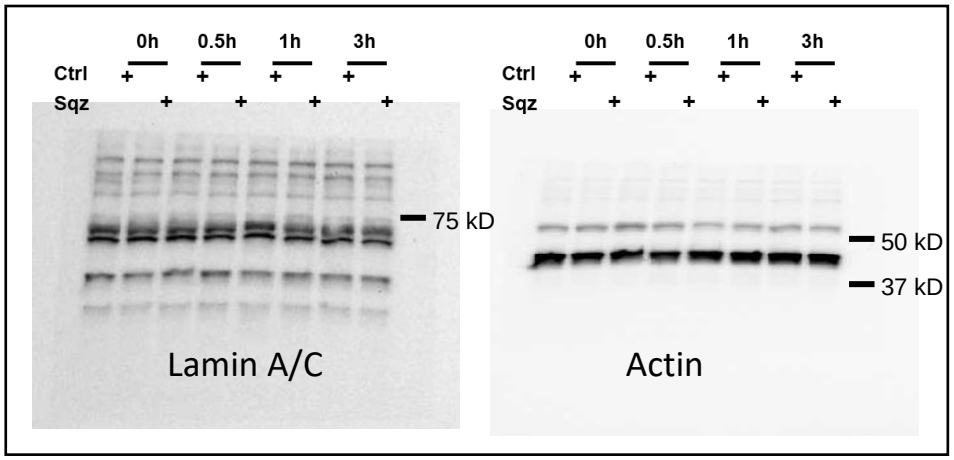

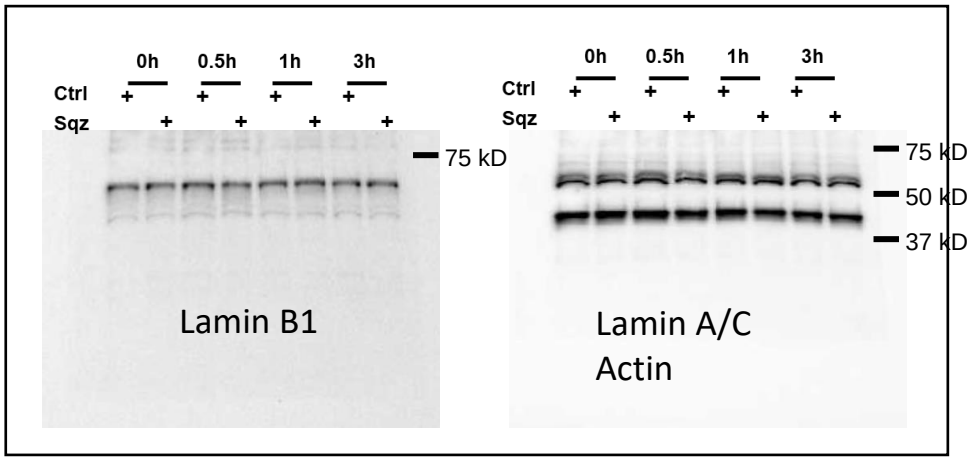

Supplementary Fig 43

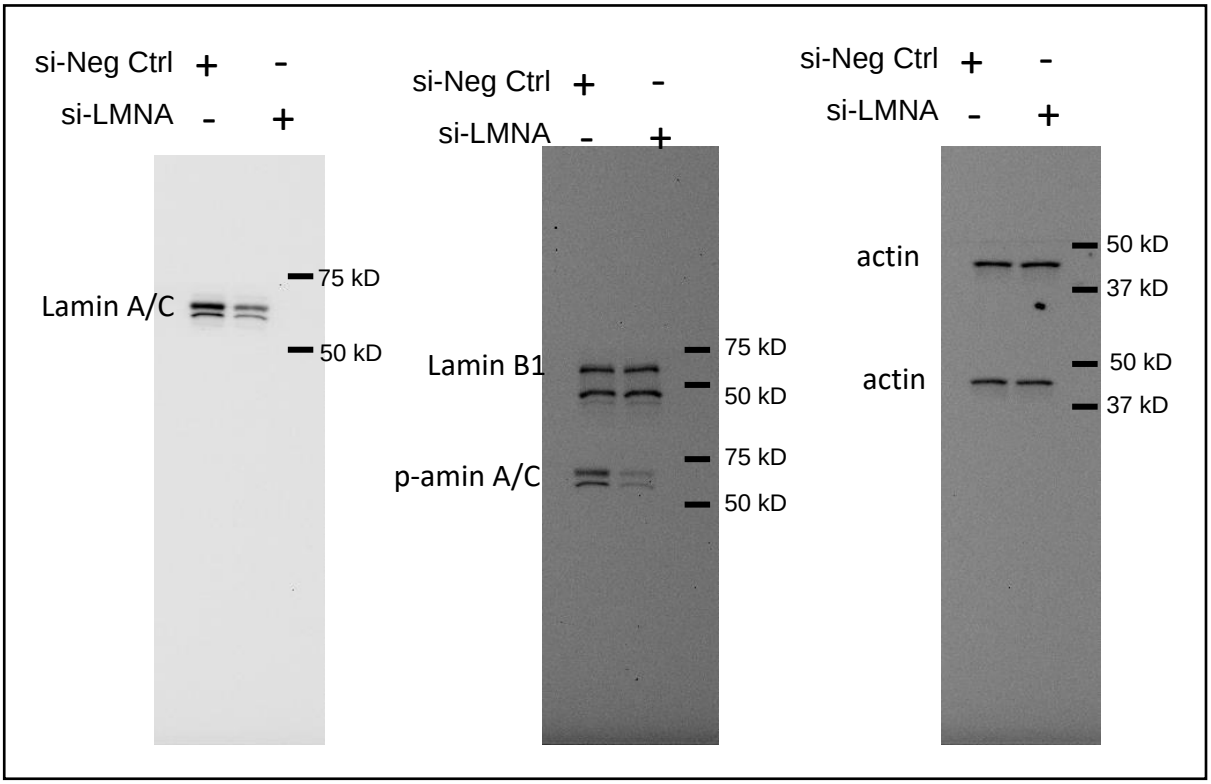

Supplementary Fig 54

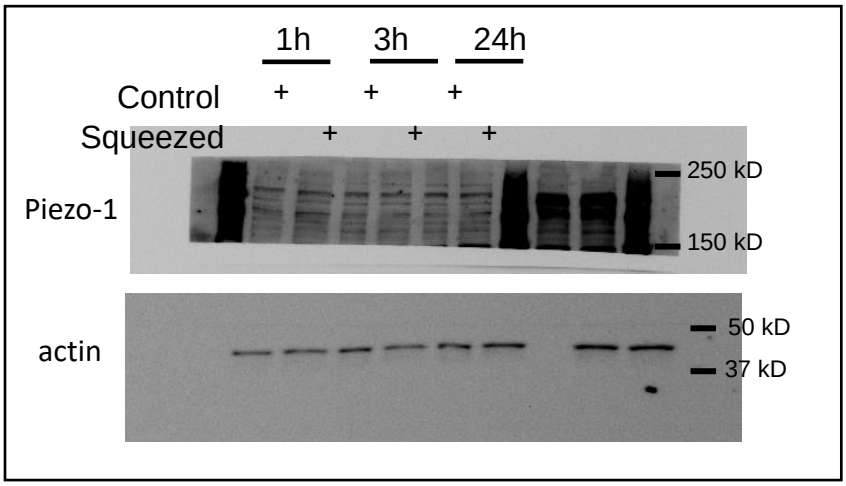

Supplementary Fig 55